

Investigating the Origin of Acoustic Signals in AE Monitoring of Stainless Steel Pitting Corrosion via Combined Electrochemical Techniques

Tongzeng Hua

2025

Faculty: Mechanical Engineering

Program: MSc in Materials Science and Engineering

Student: Tongzeng Hua Thesis Committee: Prof. Arjan Mol

> Dr. Pooria Pahlavan Dr. Axel Homborg Romain Habiyaremye

> > Date of Defense: 30th September, 2025

Contents

1	Intr	roduction	2					
2		Ekground Corrosion	3					
	2.2	2.1.2 Different types of corrosion on metals	4 5 5					
	2.3	2.2.2 Electrochemical Impedance Spectroscopy (EIS)	5 8 8					
	2.0	2.3.1 AE principles	9 9					
	2.4	Detection for pitting corrosion	12 12 15					
3	Res	search objectives	19					
	3.1	Knowledge gaps	19					
	3.2	Research questions	19					
	3.3	Novelty	19					
4	Methodology 4.1 Potential combinations of AE and Electrochemical techniques							
	4.1	Potential combinations of AE and Electrochemical techniques	20 20					
		4.1.1 AE + I otendodynamic I dialization (I DI)	20					
		4.1.3 AE + Electrochemical Noise (EN)	20					
	4.2	Comparative Evaluation of AE and Electrochemical Combinations	20					
		4.2.1 Sensitivity to Early Corrosion Events	21					
		4.2.2 Ability to Distinguish Signal Sources	21					
		4.2.3 Perturbation of the System and Long-Term Feasibility	21					
	4.3	Signal processing	22					
		4.3.1 AE signal processing	22 22					
5	Exp	perimental	24					
	5.1	Materials and solution	24					
	5.2	AE experimental setup and parameter	24					
	5.3	EN experimental setup and parameter	24					
	5.4	Complete experimental setup	24					
6	Res	sults and discussion	2 6					
	6.1	Photos of experimental setup after experiment	26					
	6.2	Optical Microscopy	26					
	6.3	AE results	28					
	6.4	EN results	33					
	6.5	6.4.1 EN raw data	33 37					
7		nclusions	44					
8	кес	commendations for future research	45					

1 Introduction

Corrosion represents a critical issue worldwide, with profound economic, environmental, and safety consequences. The degradation of materials in industrial and infrastructure settings leads to enormous maintenance and replacement costs annually. According to the 2016 IMPACT study by NACE International, the global cost of corrosion was estimated at approximately US\$2.5 trillion annually, equivalent to 3.4% of global GDP in 2013, with 15–35% of this cost potentially avoidable through effective corrosion management practices[1]. Beyond economic losses, corrosion has contributed to major accidents such as the 1992 Guadalajara sewer explosion and the 1999 Erika oil tanker disaster, underscoring its serious safety and environmental consequences[2]. In response, a wide range of mitigation strategies—including cathodic protection, coatings, corrosion inhibitors, and material design—have been developed to manage and prevent corrosion. Among various forms of corrosion, localized pitting is particularly insidious, as it can rapidly compromise structural components without obvious surface indication.

Stainless steel remains vulnerable to localized pitting in aggressive environments rich in chlorides or other halides, which undermine its protective oxide film. Such pits are highly localized and often hidden beneath the surface, allowing them to progress unpredictably and cause sudden failure. The sporadic initiation and subsurface growth of pits make their detection challenging until advanced stages of corrosion. Innovative monitoring approaches are therefore required to detect these corrosion damage at an early stage.

Recent advances in nondestructive monitoring have highlighted acoustic emission monitoring and electrochemical noise as powerful tools for real-time corrosion detection[3],[4],[5],[6]. AE captures transient elastic waves generated by microstructural events, such as crack formation, and in pitting corrosion these signals may arise during pit initiation and growth[3]. EN involves the passive measurement of spontaneous fluctuations in electrical current or potential from corrosion reactions on the metal surface[7]. As both AE and EN can continuously monitor the corroding system without interference, they offer significant advantages over conventional inspection methods.

However, a fundamental knowledge gap remains regarding the physical origins of AE signals during pitting corrosion. Various hypotheses have been proposed, including localized metal cracking, passive film rupture, or hydrogen gas evolution[8],[9],[10],[11],[12]. But no definitive consensus has been reached. Resolving these ambiguities is essential for reliable interpretation of AE data. This thesis combines acoustic emission with electrochemical noise in a synchronized, open-circuit framework to investigate pitting corrosion of AISI 304 stainless steel in aggressive chloride media. By time-aligning AE with ENdefined activity windows and applying appropriate signal processing to both channels, the study seeks to correlate acoustic fingerprints with electrochemical transients and to discriminate film rupture type events and hydrogen bubble events. This helps to clarify AE source mechanisms and to advance AE+EN as a practical way for early warning and mechanistic mapping of pitting corrosion.

2 Background

2.1 Corrosion

2.1.1 Fundamentals of corrosion

The definition of corrosion is given as the destructive attack of a metal in its environment by electrochemical or chemical reactions with oxygen, water, chlorine, sulfur and other aggressive species[13]. When a metal comes into contact with an electrolyte, electrochemical corrosion happens. This process has two reactions happening at the same time: The metal loses electrons and starts to dissolve at the anode, while the reduction reaction happens at the cathode, often producing hydrogen gas[14]. The anode, the cathode and electrolyte are the three essential parts for electrochemical corrosion to happen[15]. The electrolyte serves as an electrically conductive medium to form a circuit, with the anode acting as the site of metal corrosion, while the cathode may be located on the same metal surface or on a different metal immersed in the electrolyte.

At the anodic site, the metal electrode undergoes dissolution. It releases positively charged ions into the electrolyte and generates electrons that are consumed at the cathodic site, as shown in equation(1). Consequently, the corrosion current consists of electron flow through the metal and ion migration within the electrolyte[15]. These half-cell reactions are thought to take place at numerous microscopic anodes and cathodes distributed across the corroding surface, leading to material degradation over time. The electrochemical processes that occur at the anodic and cathodic sites are illustrated in the reactions below[16],[17]:

Anodic reaction:

$$M_{(s)} \longrightarrow M_{(aq)}^{n+} + n e^-$$
 (1)

Cathodic reaction:

(A) Oxygen reduction (acid solution)

$$O_{2(g)} + 4H^+ + 4e^- \longrightarrow 2H_2O$$
 (2)

(B) Oxygen reduction (neutral or basic solution)

$$O_{2(g)} + H_2O_{(l)} + 2e^- \longrightarrow 2OH^-$$
 (3)

(C) Hydrogen evolution (acid solution)

$$2 H_{(aq)}^{+} + 2 e^{-} \longrightarrow H_{2(g)}$$
 (4)

(D) Metal ion reduction: metal ions present in the electrolytic solution may be reduced:

$$\mathbf{M}^{n+} + \mathbf{e}^{-} \longrightarrow \mathbf{M}^{(n-1)+} \tag{5}$$

Metal ion reduction occurs only if M^{n+} ions are in high concentration. Here, the M^{n+} ions decrease their valence state by accepting an electron.

(E) Metal deposition: metal may be reduced from its ionic form to a neutral metallic form:

$$M^{n+} + e^{-} \longrightarrow M_{(s)}$$
 (6)

2.1.2 Different types of corrosion on metals

There are different types of corrosion shown in Figure 1 including uniform corrosion, pitting corrosion, galvanic corrosion, stress corrosion cracking, crevice corrosion, corrosion fatigue, intergranular corrosion. Corrosion can be classified as general corrosion and localized corrosion[18]. In this section, pitting corrosion is to be focused on.

General corrosion is also known as uniform corrosion, during which electrochemical reactions take place uniformly across a wide area of the exposed metal surface when in contact with aqueous or atmospheric media[19]. It can be characterized by a consistent corrosion rate over the unprotected surface. Oxygen is the main contributing factor to this type of corrosion. Common materials susceptible to general corrosion include cast iron and carbon steel when exposed to a humid environment. They will typically develop a rust-like appearance[20].

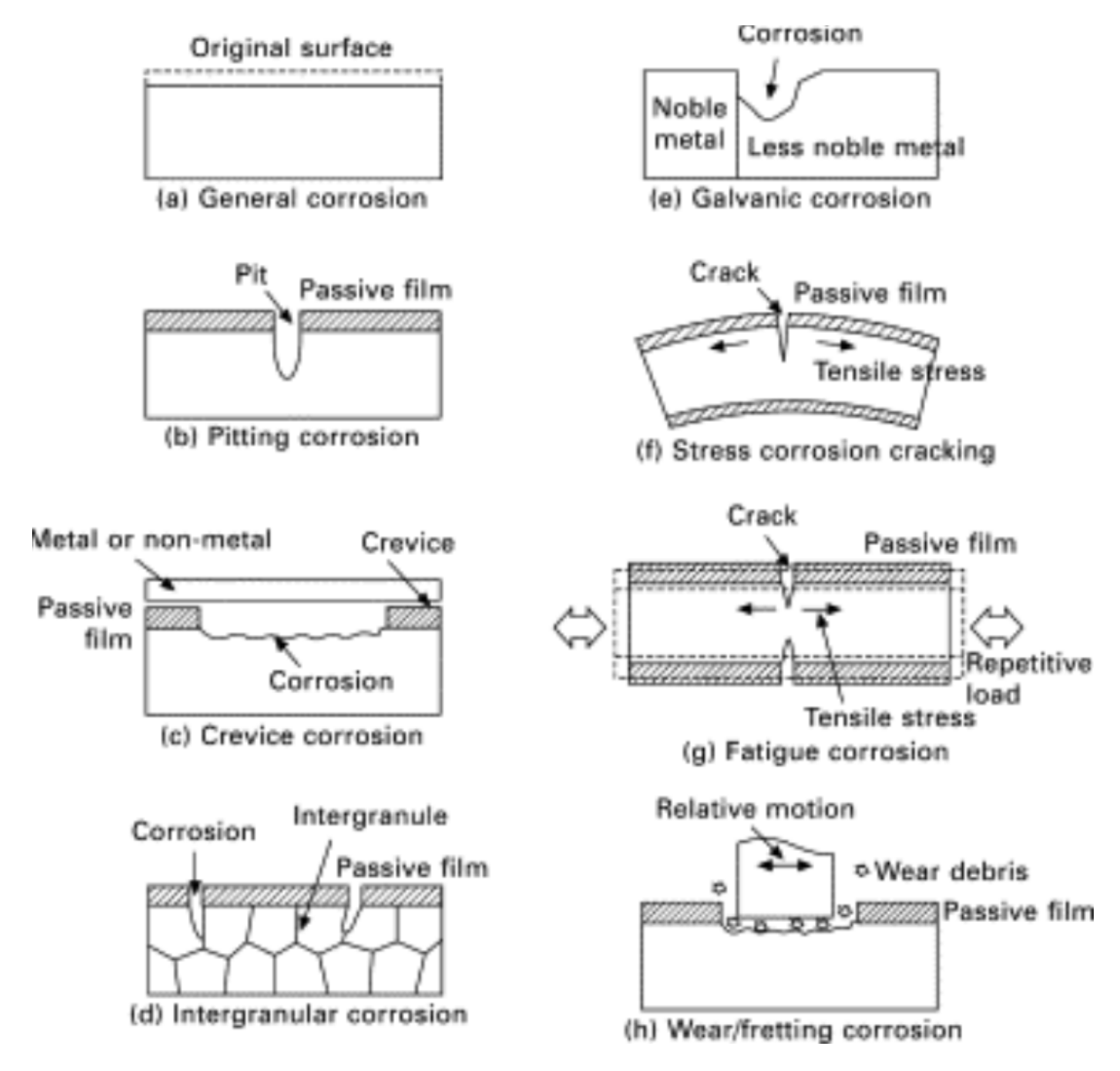


Figure 1: Different types of corrosion[21]

Localized corrosion refers to the intensified degradation of a passive metal at specific sites where the protective passive film has deteriorated in an otherwise corrosive environment[22]. Compared to general corrosion, localized corrosion is more dangerous, harder to predict and to detect and it may cause sudden and severe failures[23].

Localized corrosion can manifest in various forms, including pitting on openly exposed metal surfaces, crevice corrosion occurring in confined regions shielded from the surrounding environment, and intergranular corrosion in alloys with vulnerable grain boundaries[24].

Crevice corrosion refers to the localized attack that takes place in narrow, confined regions on a metal surface where exposure to the external environment is limited. These confined zones are known as crevices[25]. Within the crevice, the transport of metal ions generated by anodic reactions is hindered,

resulting in their accumulation in the confined space. This localized increase in metal ion concentration promotes hydrolysis with water, leading to a significant drop in pH. The resulting acidic environment accelerates corrosion beneath the crevice, often making it more severe than on exposed surfaces [26].

Wear corrosion occurs when mechanical loading leads to repetitive damage and removal of the passive film on metallic surfaces. This exposes the underlying bare metal to the environment, accelerating local corrosion processes[27]. This phenomenon is particularly critical in biomedical implants, where wear corrosion often takes place at contact interfaces, such as the head-stem junction in joint prostheses and screw-hole regions in bone plates[28],[29].

Pitting corrosion results from the localized breakdown of the passive film on a metal surface, leading to the formation of deep, narrowly confined pits. This phenomenon commonly occurs in passivated metals exposed to aqueous environments containing dissolved salts[30]. It involves the localized and rapid dissolution of metal following the breakdown of its passive protective film. Anions from dissolved salts, particularly chloride ions, can disrupt the stability or regeneration of the passive layer, thereby initiating and propagating pit formation on the metal surface[19],[31]. As illustrated in Figure 2, pitting corrosion induced by chloride ions is autocatalytic in nature, which means that the localized environment created during pit formation further enhances the corrosion process. Within the pit, the steel undergoes dissolution, attracting chloride ions toward the resulting positive charge. The metal chlorides formed subsequently undergo hydrolysis, producing insoluble metal hydroxides and hydrochloric acid[23]. This process will finally result in a significant drop in pH within the localized environment and accelerate pitting corrosion further.

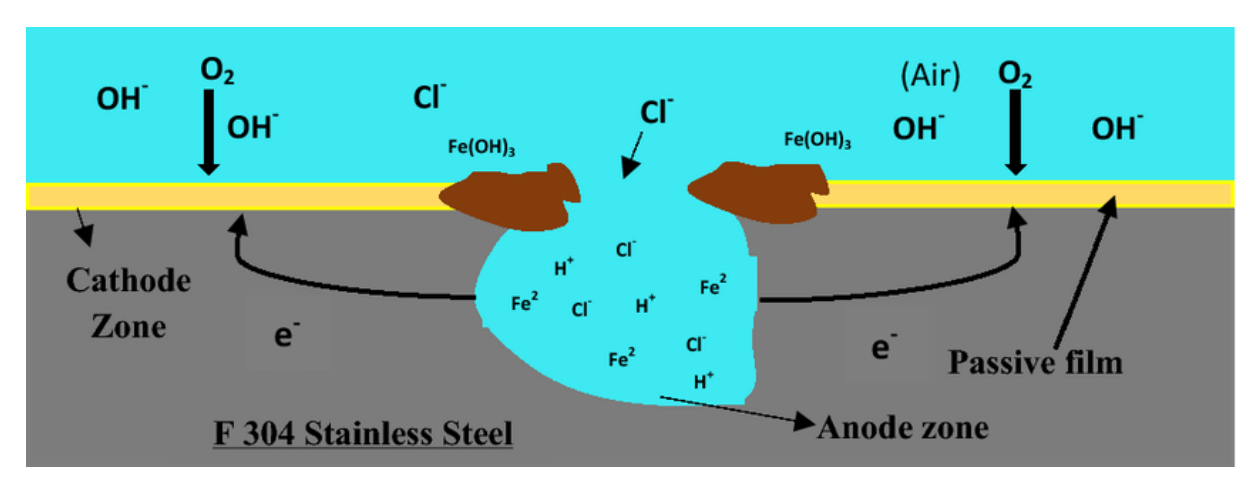


Figure 2: Mechanism of pitting corrosion[32]

2.2 Corrosion monitoring

2.2.1 Potentiodynamic polarisation

Potentiodynamic polarization is an electrochemical method in which the potential of a working electrode is swept (usually from more negative to more positive relative to the open circuit potential) at a controlled scan rate, while the resulting current density is recorded. From the resulting polarization curve one can extract key corrosion parameters such as the corrosion potential, corrosion current density, and Tafel slopes. These parameters allow quantitative estimation of corrosion rates, assessment of passivation behaviour, determination of pitting or breakdown potential, and comparison of the influence of environmental conditions or material treatments on corrosion behaviour. The accuracy of the extracted parameters depends critically on experimental conditions such as scan rate, electrolyte composition, and the existence of well-defined Tafel regions[33].

2.2.2 Electrochemical Impedance Spectroscopy (EIS)

In a typical electrochemical cell, the interactions between redox-active species and the electrode involve several key factors, including the concentration of electroactive species, charge transfer kinetics, mass transport from the bulk solution to the electrode interface, and the intrinsic resistance of the electrolyte. Each of these features can be represented by an equivalent electrical circuit composed of resistors, capacitors, and constant phase elements, which are arranged in series or parallel configurations to model

the electrochemical behavior of the system.[34] This is illustrated in Figure 3. Therefore, EIS can be employed to investigate mass transport, charge transfer, and diffusion phenomena. It serves as a powerful tool for probing intrinsic material properties and specific interfacial processes that influence the conductivity, resistance, or capacitance of an electrochemical system.[35] Unlike direct current resistance, which follows Ohm's law directly, impedance reflects the opposition to alternating current and accounts for both resistive and reactive components. In EIS, a small amplitude sinusoidal voltage is applied to the system. The resulting current response, which is also sinusoidal at the same frequency, exhibits a phase shift. Under these conditions, the electrochemical response can be approximated as pseudo-linear. This allows impedance to be quantified as a frequency-dependent complex function[35].

The applied excitation voltage is expressed as a time-dependent sinusoidal function, as illustrated in Equation (7)[35]:

$$E_t = E_0 \cdot \sin(\omega t) \tag{7}$$

where E_t is the instantaneous potential at time t, E_0 is the amplitude of the applied signal, and ω is the angular frequency (in radians per second).

The applied frequency f can be expressed as the angular frequency ω when using radians per second rather than hertz, as given by Equation 8:

$$\omega = 2\pi f \tag{8}$$

In a linear system, the current response is phase-shifted by an angle Φ and has a different amplitude compared to the applied voltage, as shown in Equation 9:

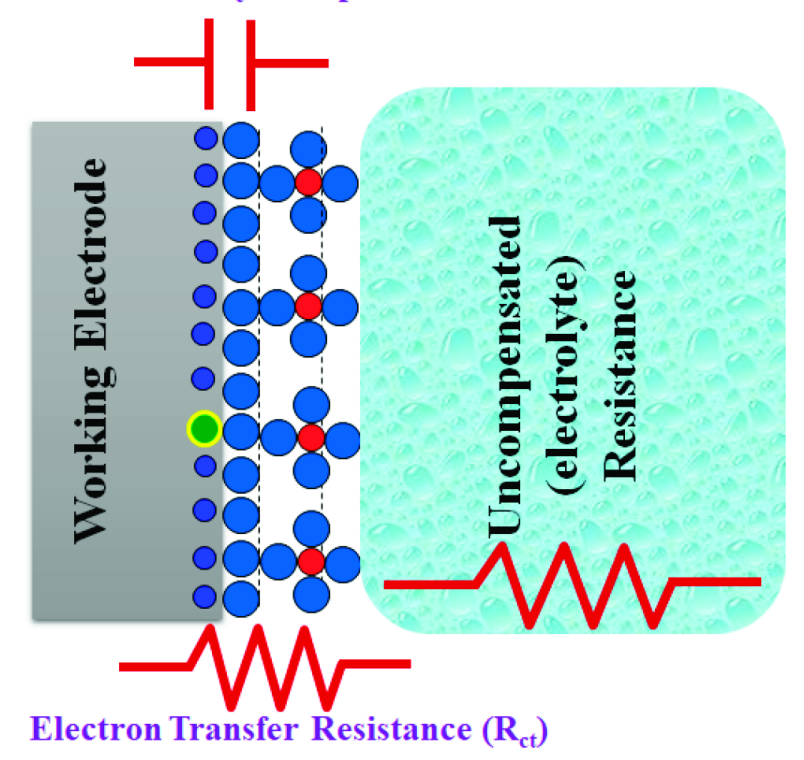
$$I_t = I_0 \sin(\omega t + \Phi) \tag{9}$$

Accordingly, the impedance of the system can be expressed as:

$$Z = \frac{E}{I} = Z_0 \exp(i\Phi) = Z_0 (\cos \Phi + i \sin \Phi)$$
(10)

Here, Z, E, I, ω , and Φ denote the impedance, voltage, current, angular frequency, and phase shift between E and I, respectively. Impedance is typically described by a magnitude Z_0 and a phase angle Φ . When the applied sinusoidal voltage is plotted along the X-axis and the corresponding current response is plotted along the Y-axis, the resulting figure is known as a 'Lissajous plot', as shown in Figure 4. Prior to the development of modern EIS instruments, Lissajous analysis was the primary method for measuring impedance [34],[36]. Modern instrumentation enables fully automated application of a voltage perturbation with a controlled, variable frequency while simultaneously recording the resulting impedance and current responses. During the frequency sweep—from the megahertz or gigahertz range, where the signal time scale is on the order of micro- to nanoseconds, down to the microhertz range, corresponding to time scales of several hours—the measured data are plotted as the imaginary versus real components of the impedance, yielding a complex impedance representation commonly referred to as a Nyquist plot[37].

Double Layer Capacitance



 $\begin{array}{c} R_{ct} \\ \hline \\ R_{s} \end{array}$ Randles Cell (Simplified)

Figure 3: A simplified scheme to represent the EIS equivalent circuit and the redox processes occurring at the surface of the working electrode in a conventional three-electrode electrochemical cell. $R_{\rm ct}$ denotes the charge transfer resistance, $R_{\rm s}$ represents the electrolyte (solution) resistance, and $C_{\rm dl}$ corresponds to the double-layer capacitance[34].

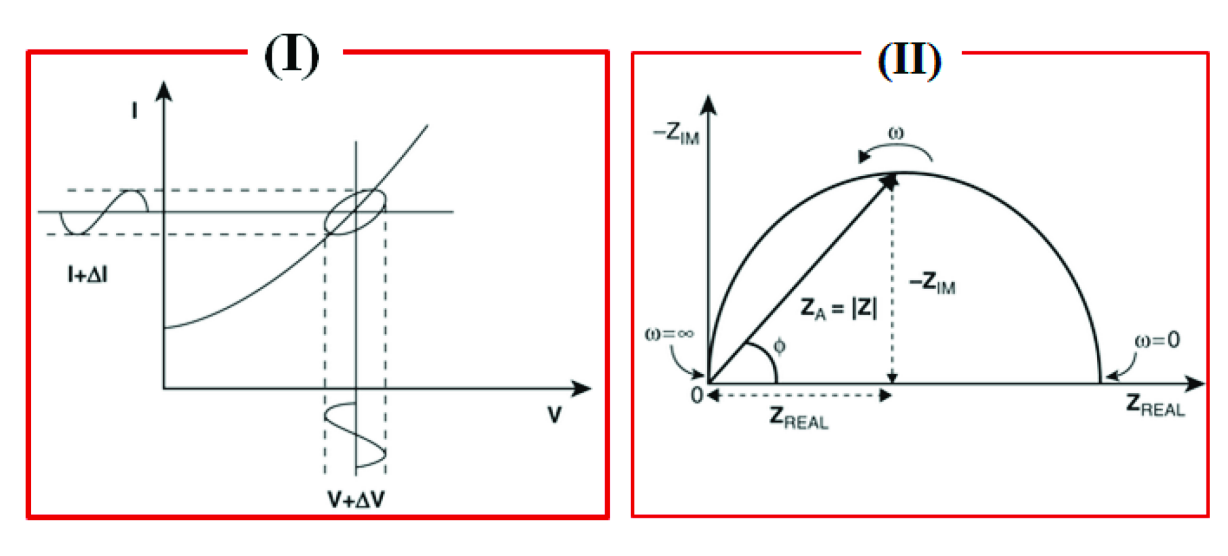


Figure 4: I:the Lissajous plot, II: the Nyquist plot[37]

2.2.3 Electrochemical noise(EN)

Electrochemical noise (EN) refers to the spontaneous low-amplitude fluctuations in potential and current that arise from the charge transfer reactions during ongoing electrochemical processes[38]. In a corroding metal system, random transient events, such as the initiation and re-passivation of metastable pits or discrete bursts of cathodic reactions exist. This could induce measurable perturbations in electrode potential and coupling current. EN measurements are typically performed using two nominally identical working electrodes (to measure current noise between them) and a reference electrode (to measure potential noise) in a zero-resistance ammeter setup[39]. Under open circuit conditions, any localized anodic event on one electrode and its corresponding cathodic counterpart on the other will produce a current flow between the electrodes and a shift in their potentials. Thus, the nature of the noise signals such as magnitude and (localized) frequency of transients can reflect the underlying corrosion mode.

2.3 Acoustic emission

2.3.1 AE principles

Acoustic emission typically monitors the propagation of elastic waves, which are induced by the sudden release of energy from localized sources within the material [40]. These signals are usually ultrasonic waves. These emissions usually originate from events such as crack initiation and growth, dislocation movements, phase transformations, or corrosion-related processes [41]. With the help of an acoustic emission sensor, these high-frequency elastic waves are converted into electrical signals. The piezoelectric materials in the sensor deform in response to incoming stress waves, producing a voltage proportional to the wave's amplitude. This allows for the detection and analysis of events. AE sensors are usually directly contacted with the material surface. These piezoelectric AE sensors can be broadly classified into two categories [42]. One is bulk acoustic wave sensors, which detect all types of acoustic emission waves. The other is surface acoustic wave sensors, which are specifically designed to detect Rayleigh surface waves and are the most commonly used type. Figure 5 shows the different wave types during propagation of acoustic emission signals. A pre-amplifier is usually used after the AE sensor to amplify the signals. Figure 6 illustrates a typical experimental setup of AE for

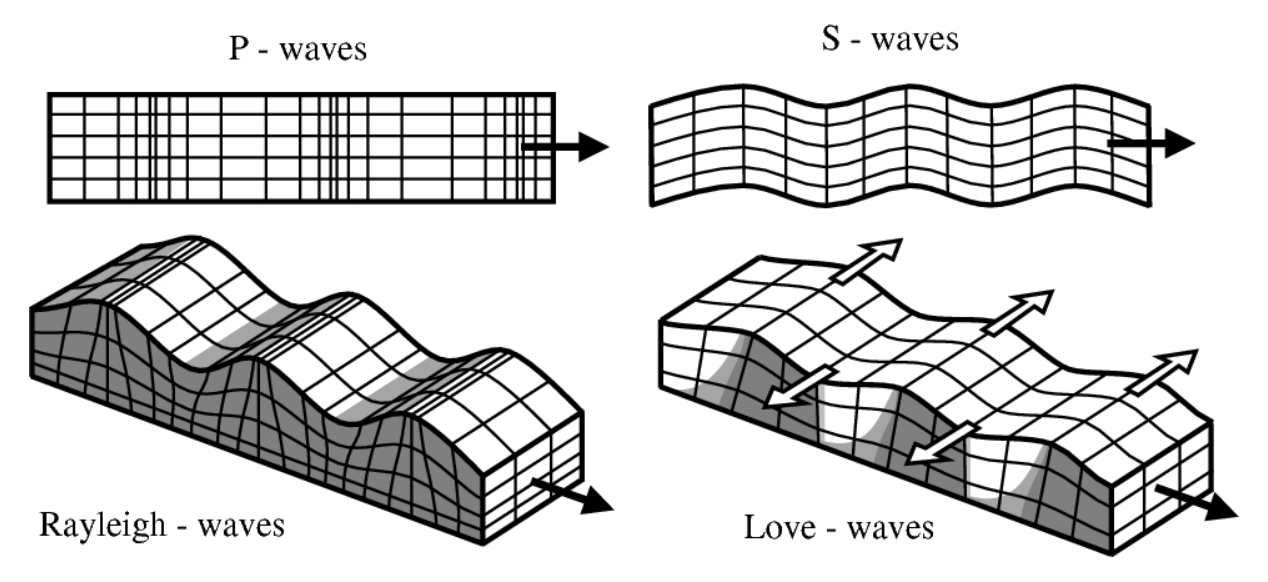


Figure 5: The wave type during propagation of acoustic emission signals [43]

2.3.2 AE parameters

The examination of acoustic emission waveforms is recognized as a simple but reliable approach for characterizing and distinguishing different AE sources[45]. Figure 7 illustrates the typical measurement parameters commonly used to characterize an acoustic emission signal waveform.

The following is the definition of these parameters[44]:

Amplitude: Amplitude (A) is the highest peak of the measured voltage signal and it is measured in decibels (dB). This is an important parameter in NDT inspection since it determines the signal detectability.

Threshold: The threshold is a predefined setting used to filter out electronic and environmental background noise. Only acoustic emission (AE) signals with amplitudes exceeding this threshold are captured. While higher threshold values effectively minimize the likelihood of recording noise, it is essential to strike a balance to avoid excluding weak but potentially meaningful AE events that may be masked by low-amplitude background signals.

Duration: Duration (D) refers to the time span between the initial and final crossings of the threshold by the signal waveform. It indicates the length of time that an acoustic event is considered relevant.

Risetime: Risetime (R) is defined as the time elapsed between the initial threshold crossing and the point at which the signal reaches its peak amplitude. This parameter is associated with the propagation characteristics of the acoustic emission (AE) wave from its source to the sensor.

Energy: Energy (E) is defined as the integral of the area under the envelope of the acoustic emission (AE) voltage signal waveform.

Counts: Counts (CNT or N) represent the number of times the signal amplitude exceeds the predefined threshold. This parameter is influenced by the intensity of the AE event, the resonant behavior of the sensor, and the properties of the material under inspection. Although counts alone do not provide detailed information about the event's nature, when analyzed in conjunction with amplitude and/or duration, they can still offer insights into the overall shape of the AE waveform.

Average frequency: Average Frequency (AF or AVG) is an indirect parameter derived from the AE waveform. It is defined as the ratio of the total number of counts to the signal duration.

RA value: The ratio between risetime and amplitude defines the RA value. It serves as a useful parameter for characterizing crack modes. By connecting with average frequency, it enables the classification of acoustic emission signals associated with tensile or shear fracture behaviour.

2.3.3 AE source mechanisms

There are some possible mechanisms that are believed to be potential sources of AE during corrosion. Yuyama et al. presented a schematic overview of the potential acoustic emission sources that might be detected during stress corrosion cracking or corrosion fatigue processes[46]. As illustrated in Figure 8, various phenomena contribute to AE activity during these stress-assisted corrosion mechanisms. The primary sources include crack initiation and propagation, hydrogen bubble formation from cathodic

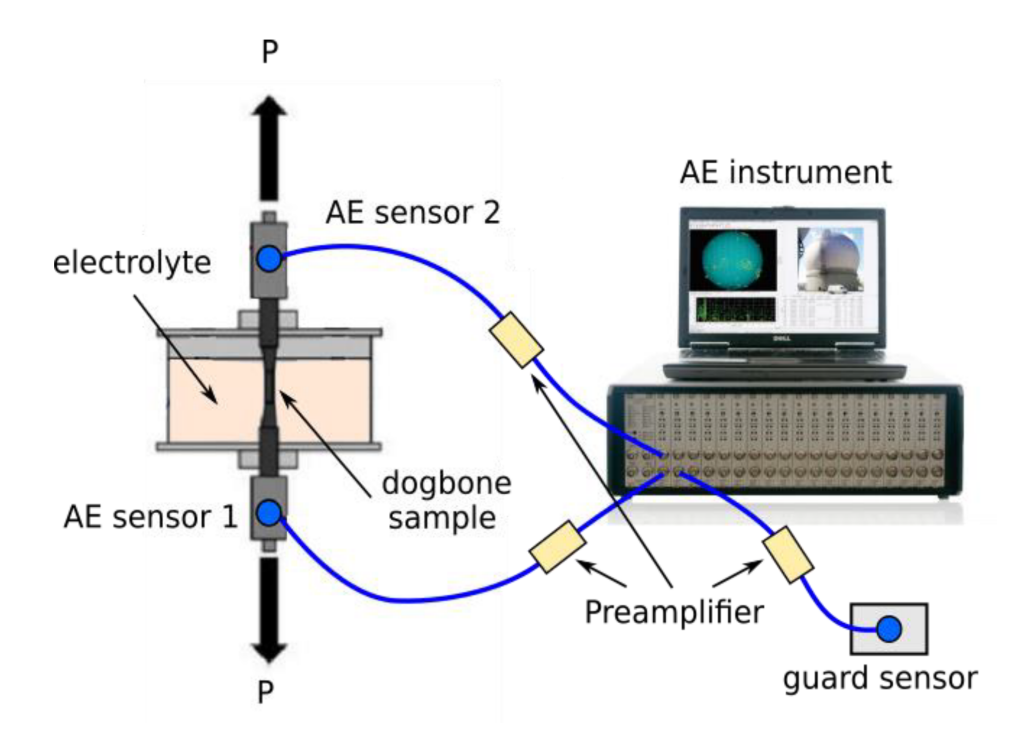


Figure 6: Schematic of AE setup[44]

reactions, and the rupture of thick surface oxide films. Localized AE sources at the crack tip plastic zone may also arise from slip deformation, twinning, or the fracture and decohesion of precipitates, second-phase particles, and nonmetallic inclusions[44].

In the case of pitting corrosion, the exact mechanisms responsible for AE signals remain unclear and inconclusive. Most current studies suggest that hydrogen bubble activity is the primary source of AE signals during the pitting process. These signals may arise from bubble formation[8],[10],[11], release from the pit[8], collapse[47], or physical interactions between the bubbles and the pit walls, such as impact or friction[9],[12]. However, other physical processes have also been proposed as potential sources of AE, such as the rupture of the salt film[48], the breakdown of the pit cover[49], the cracking of corrosion products[50] and the disruption of the passive film[51].

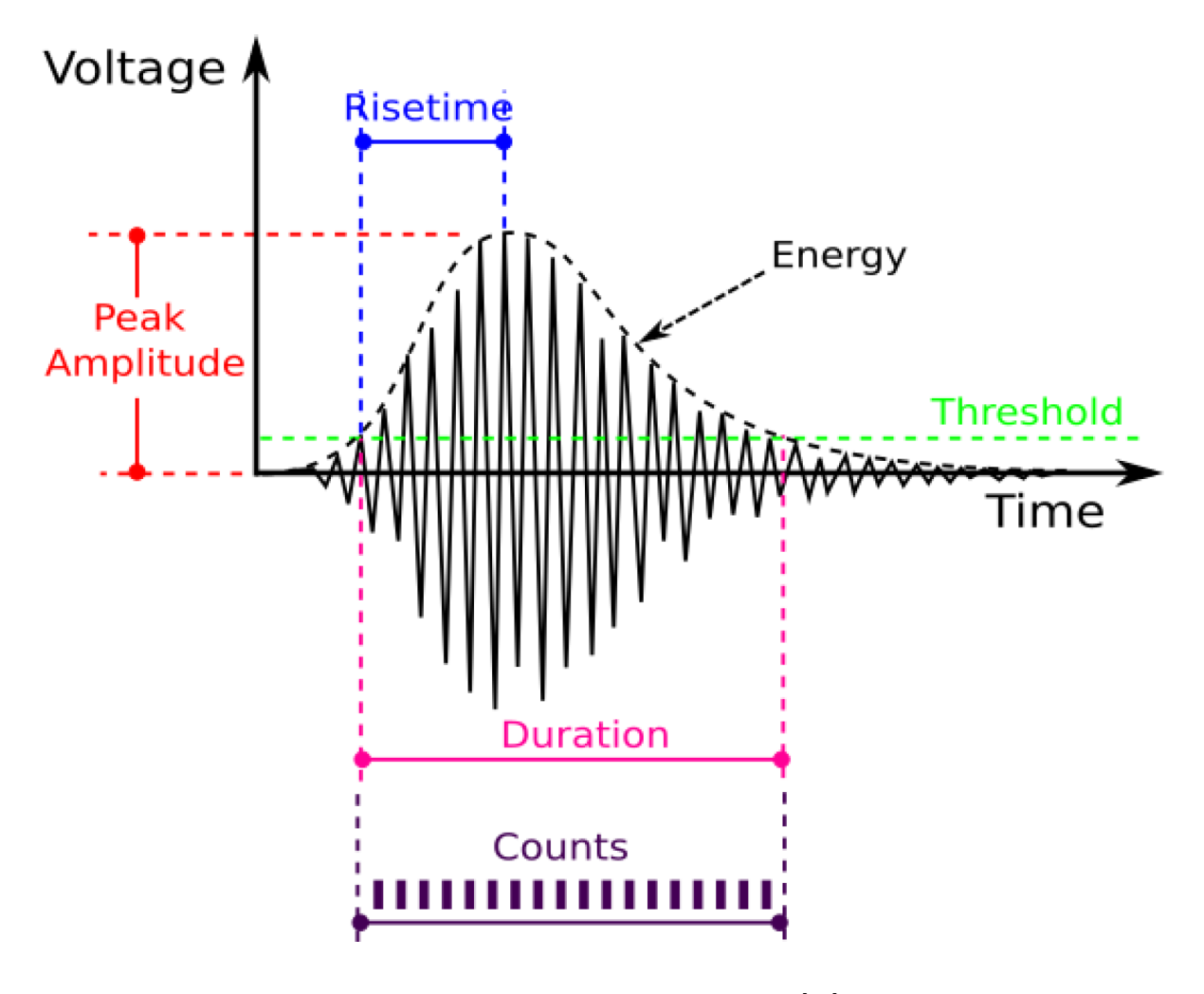


Figure 7: Acoustic emission parameters [44]

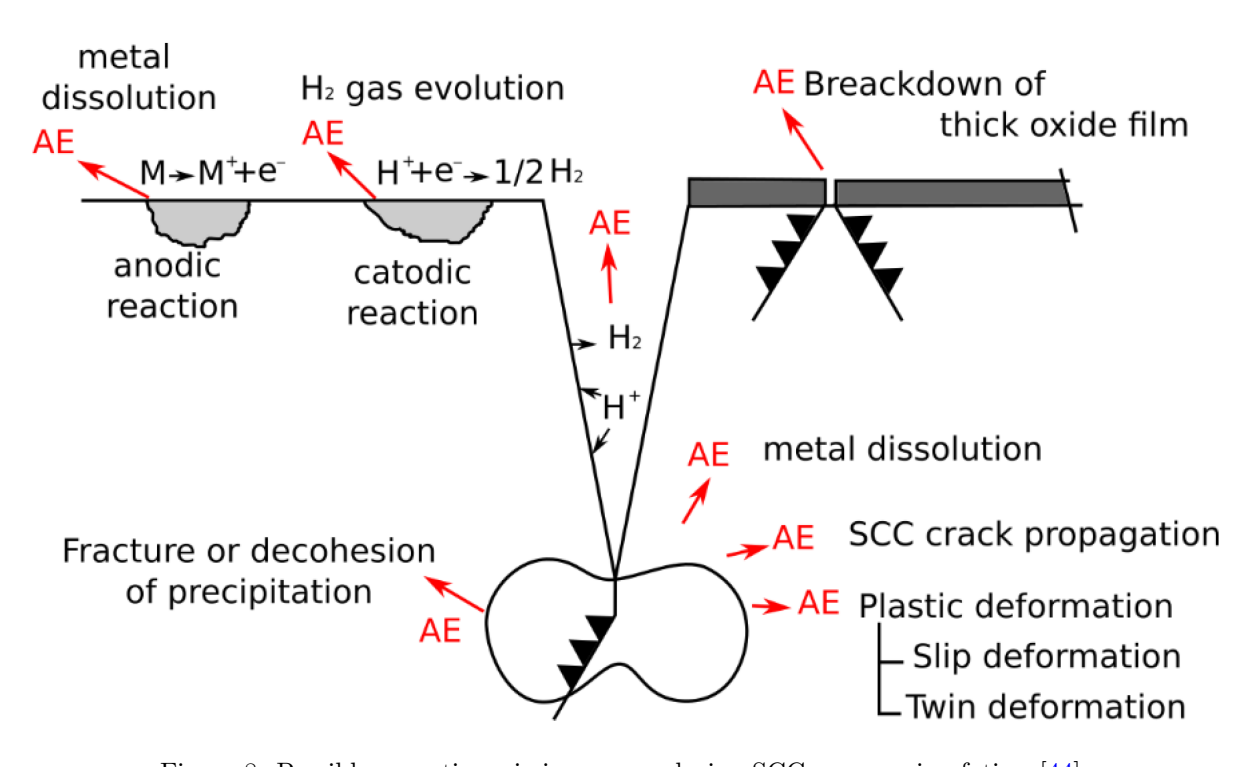


Figure 8: Possible acoustic emission source during SCC or corrosion fatigue [44]

2.4 Detection for pitting corrosion

Electrochemical monitoring methods provide quantitative and mechanistic insights into corrosion processes by measuring electrical responses of the metal/electrolyte interface. For pitting corrosion of stainless steels, several electrochemical techniques are particularly informative: electrochemical impedance spectroscopy (EIS) can detect changes in passive film properties and pit growth, electrochemical noise (EN) analysis captures spontaneous transient events associated with pit initiation, and potentiodynamic polarization tests identify the critical potentials at which pits nucleate or repassivate. Each of these techniques has been applied both in standalone studies of pitting and in combination with AE. This section briefly reviews the principles and state-of-the-art usage of EIS, EN, and potentiodynamic polarization for pitting corrosion monitoring.

2.4.1 Electrochemical Techniques for Pitting Corrosion Monitoring

Electrochemical Impedance Spectroscopy (EIS) for Pitting Detection

Researchers have developed EIS-based strategies to identify the stages of pitting. For instance, dynamic EIS, where impedance spectra are recorded continuously while the electrode potential is swept, can capture the transition from passive to pitting states. In 2017 Orlikowski et al. used this approach to study 304L stainless steel in chloride solution[52]. They observed distinct impedance signatures corresponding to (i) the passive state, (ii) metastable pitting (film breakdown events that had not yet grown into stable pits), and (iii) stable pitting corrosion[52]. In the metastable pitting range, the impedance data still showed a capacitive behavior dominated by the passive film response, albeit with gradually decreasing resistance, indicating that the pits were nucleating but quickly repassivating (an activationcontrolled process[52]. Once the potential increased into the stable pitting regime, a more drastic drop in charge transfer resistance was seen, and an additional low-frequency time constant appeared in the impedance spectrum [53]. This extra time constant was attributed to processes inside the pits (such as mass transport of ions in the pit or faradic reactions on the pit surface) that are absent when the surface is uniformly passive [53]. In short, EIS could distinguish the pit initiation period from the pit propagation period by the changes in the measured impedance spectra. It is valuable because this allows researchers to detect that pitting has started (even if only metastably) before it might be obvious from a simple DC measurement.

Another use of EIS is to monitor the progression of pitting over time at a fixed potential or open-circuit. For example, after a certain exposure time or after an applied perturbation (like cyclic polarization), impedance measurements can be taken to see how much the passive film has degraded. A significant reduction in low-frequency impedance or the appearance of an inductive loop (often associated with adsorption/desorption of intermediates or relaxation of localized corrosion processes) can indicate that pits have formed. In one study on a novel high-alloy steel, an inductive behavior in the low-frequency EIS was correlated with pitting at the particle–matrix interfaces and the localized attack was later confirmed by microscopy[54] as shown in Figure 9 and Figure 10.

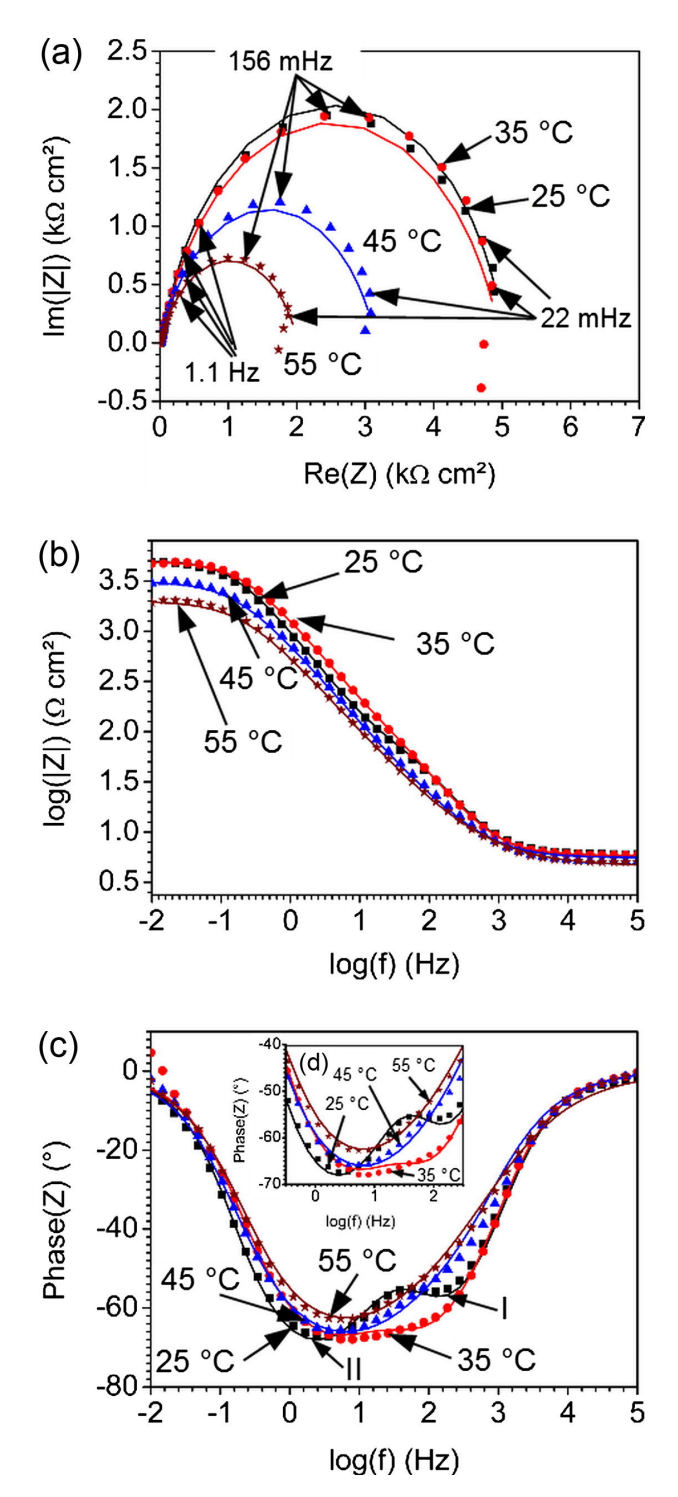


Figure 9: EIS results of spark plasma sintered particle-reinforced CrMnNi steel recorded at various temperatures following cyclic polarization. (a) Nyquist plot; (b) and (c) corresponding Bode magnitude and phase angle plots[54].

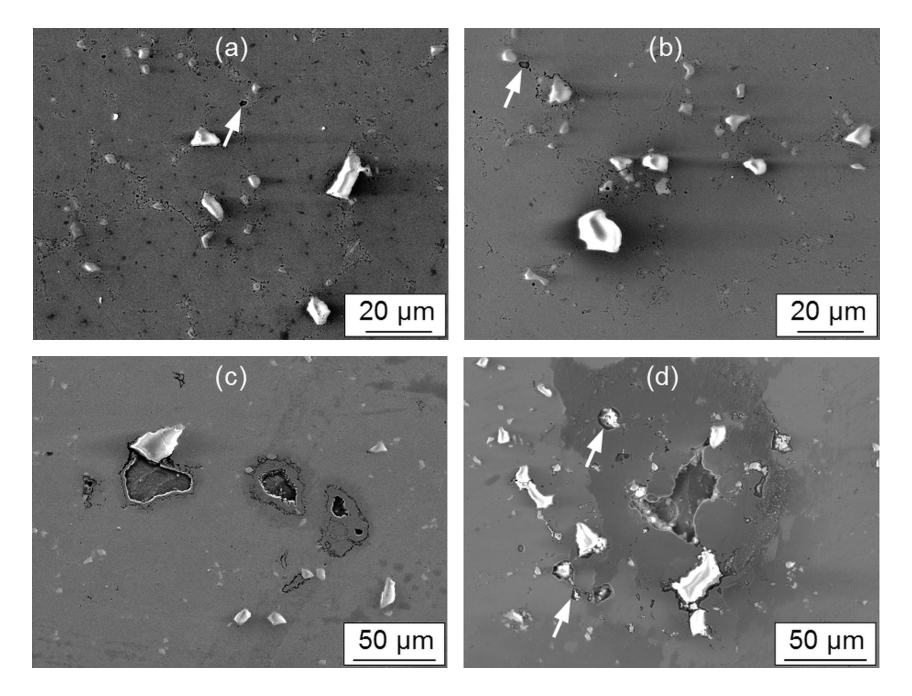


Figure 10: SEM of the surface morphology after cyclic voltammetry in 5 wt.% NaCl solution at different temperatures: (a) 25 °C; (b) 35 °C; (c) 45 °C; and (d) 55 °C[54].

Electrochemical Noise (EN) for Pitting Corrosion Monitoring

Electrochemical noise (EN) techniques have emerged as a promising non-intrusive method to monitor corrosion in situ by measuring spontaneous fluctuations in potential and current during the corrosion process[38]. Unlike conventional electrochemical methods that impose external perturbations, EN relies on the natural "fingerprint" of corrosion events. Researchers have been exploring EN for decades as a sensitive indicator of localized corrosion, including pitting, in various metals and environments[55].

For example, Hladky and Dawson showed that monitoring electrochemical noise enables detection of pitting and other forms of localized attack in steels[56]. In a subsequent study, they observed characteristic 1/f spectral behavior in corrosion noise, linking it to corrosion processes[57]. These pioneering works indicated random fluctuations in a corrosion system are not mere background nuisance, but carry meaningful information about the kinetics and type of corrosion occurring.

Two fundamental quantities often extracted from EN data are the noise resistance (R_n) and the localization index (LI). The noise resistance is defined analogously to polarization resistance as the ratio of the standard deviations of potential and current noise $(R_n = \sigma_V/\sigma_I)[38]$. In theory, R_n can correlate with the corrosion rate for general corrosion and EN measurements for uniform corrosion often agree with conventional DC or AC techniques[39]. The localization index is a parameter intended to indicate the likelihood of localized vs. uniform corrosion; it is often computed from the relative magnitudes of current noise compared to the total charge or using the ratio of noise resistance to polarization resistance[38]. A high LI suggests that most of the corrosion current is arising from transient localized events, whereas a low LI would correspond to uniform corrosion where current is evenly distributed[38]. In practice, values of LI, as well as statistical measures of the noise signal such as skewness and kurtosis of the current distribution, have been correlated with different corrosion types[38].

Cottis developed a simulation model treating pitting events as random pulses of charge to test various analysis criteria for EN data[39]. His work proposed that the characteristic charge (average charge per pit event) and characteristic frequency (event occurrence rate) are meaningful parameters to describe pitting activity from EN signals[39]. In this simulation study, statistical parameters like skew and kurtosis emerged as useful indicators of localized corrosion only when the corrosion process is well-characterized, underscoring that interpretation of EN must be done cautiously[39].

Another key aspect of EN theory is dealing with drifts and trends in the data. The corrosion potential can drift over time as a result of overall changes in the surface state. This can mask the true noise[55]. Methods for detrending EN time series were developed to isolate the random noise from slower baseline changes. For example, polynomial or moving average fitting is often applied to remove trends before analysis[38]. Homborg et al. introduced time-frequency methods for trend removal to improve the extraction of meaningful noise signals from raw data[58],[55]. By separating the frequency content

associated with drift from that of actual noise, they had cleaner datasets for analysis.

2.4.2 Acoustic emission monitoring

As a passive monitoring method, one key advantage of AE is that it 'listens' to the structure continuously without the need to actively stimulate the material. Unlike ultrasound or EIS testing, there is no need to apply a signal during AE testing. This makes AE ideal for real-time health monitoring. As early as 1974 Harris and Dunegan provided one of the earliest comprehensive overviews of industrial applications of acoustic emission technology. Their work highlighted the versatility of AE in various sectors, including weld monitoring, pressure vessel inspection, and complex component testing [59]. Since then, AE has been applied in more specific corrosion mechanisms. For example, in 1995 Mazille et al. demonstrated the feasibility of using AE for real-time monitoring of pitting corrosion in AISI 316L stainless steel under controlled electrochemical conditions [60]. In that study, stainless steel samples were exposed to a chloride solution to induce pitting, and AE events were recorded concurrently. They confirmed that AE could detect the onset of pitting and subsequent pit growth, even before visible perforation occurred. Their study showed a strong correlation between the activity of the AE signal and the rate of pitting corrosion, even under low-current-density anodic polarization [60]. Around the same time, Jones and Friesel reported significant AE activity during pitting of 304 stainless steel. They concluded that these signals were not due to mechanical cracking but rather to the corrosion process itself[48]. This was an important validation that purely electrochemical damage events (such as pit nucleation) can emit detectable AE, dispelling the earlier opinions that AE in corrosion might only come from secondary cracking or other mechanical failures.

In 2001, Fregonese et al. carried out detailed AE studies to correlate specific stages of pitting with AE signatures. In one study, they monitored 316L stainless steel in a 3% NaCl solution and identified distinct AE patterns corresponding to (i) pit initiation, (ii) pit propagation, and (iii) pit repassivation[9]. During the initiation stage, only intermittent low-amplitude AE bursts were observed, which they attributed to isolated film breakage events (metastable pits). Once stable pit propagation began, the AE hit rate and energy increased markedly. This indicates continuous damage from active pit growth[9]. If a pit stopped growing, the AE activity disappeared. A follow-up study analyzed which AE signal parameters were the most representative of the pitting process, recommending that parameters such as ring-down counts and signal energy be used for quantitative correlation with pit growth[12]. These works were basic in establishing AE as a feasible method to not only detect pitting, but also to distinguish different stages of pit evolution.

Researchers have also investigated the influence of environmental factors on AE during corrosion. Xu et al. studied the behavior of AE during 304 stainless steel corrosion in acidic sulfate solutions with different pH and found that AE signals associated with transpassive dissolution (very high anodic currents causing rapid metal dissolution) could be detected in low pH media[8]. The signal amplitudes and frequencies were only weakly influenced by the applied current density or prior mechanical strain, suggesting that the AE was directly related to the corrosion reaction itself[8]. Figure11 shows the potential–pH–AE diagram based on experimental results. This study illustrates that AE can respond to different corrosion modes, from pitting to general or transpassive corrosion. Hence it gives a broad picture of the corrosion dynamics.

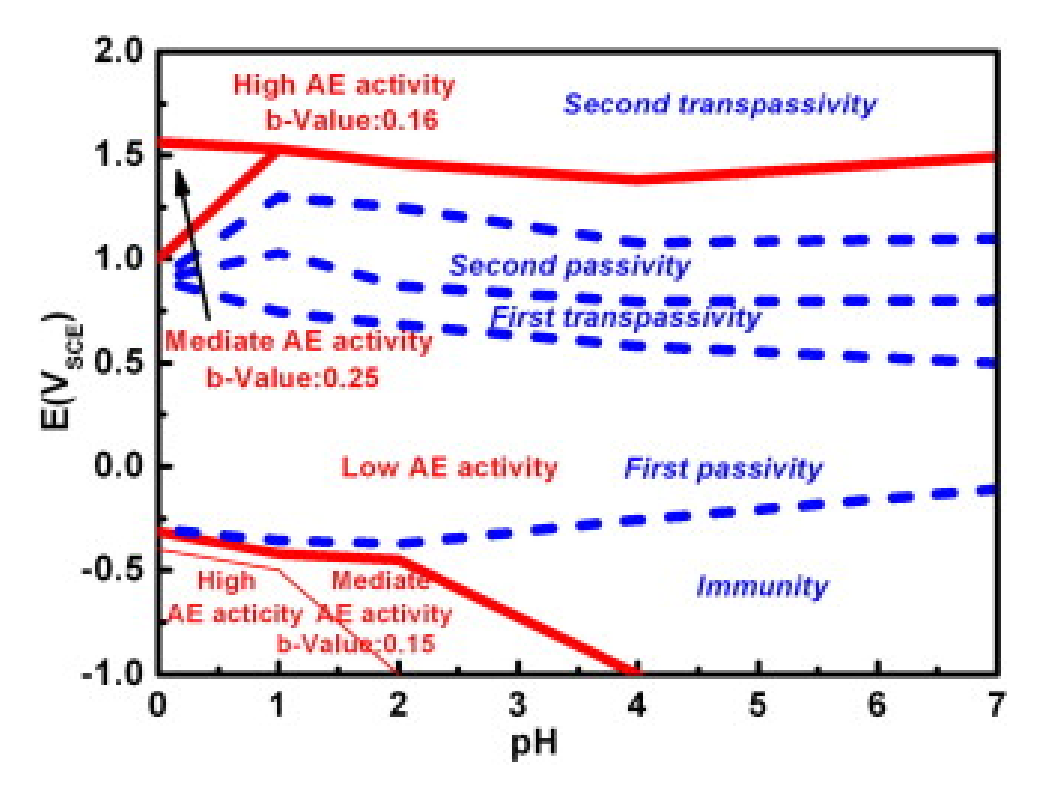


Figure 11: Diagram showing potential pH and AE results for 304 stainless steel in H_2SO_4 solutions containing Na_2SO_4 was constructed, where the dashed line represents the conventional potential–pH diagram obtained from traditional electrochemical measurements [8].

Recent experimental research has significantly improved the capabilities of in situ AE monitoring. Wu et al. introduced a novel setup to monitor the pitting in a vertically oriented 304 stainless steel sample, using AE energy as a key indicator [49]. By positioning the sample vertically, they were able to study the pitting with the influence of gravity on the pit chemistry (e.g., allowing corrosion products to partially drain). The trend in AE energy provided insight into when the pit was covered with corrosion products versus when it had an open mouth [49]. Building on this, Wu et al. specifically examined open-morphology pitting, that is, pits intentionally grown without fully adherent cover of corrosion products, and its distinct AE characteristics [61]. In that study, 304 stainless steel was prepassivated and then exposed to chloride such that pits with a clear open cavity and a separated 'tail' of corrosion product would form. They found that the AE response was strongly dependent on the morphology of the pit. Events associated with the open pit mouth had different signatures than those of the detached tail of the corrosion product below the pit [61]. By staging the corrosion process and analyzing AE at each stage, they could infer which signals corresponded to the propagation of an open pit versus the cracking or sloughing off of corrosion products in the tail. This is an important step forward, as it links AE features to the geometrical nature of the pit, not just its existence.

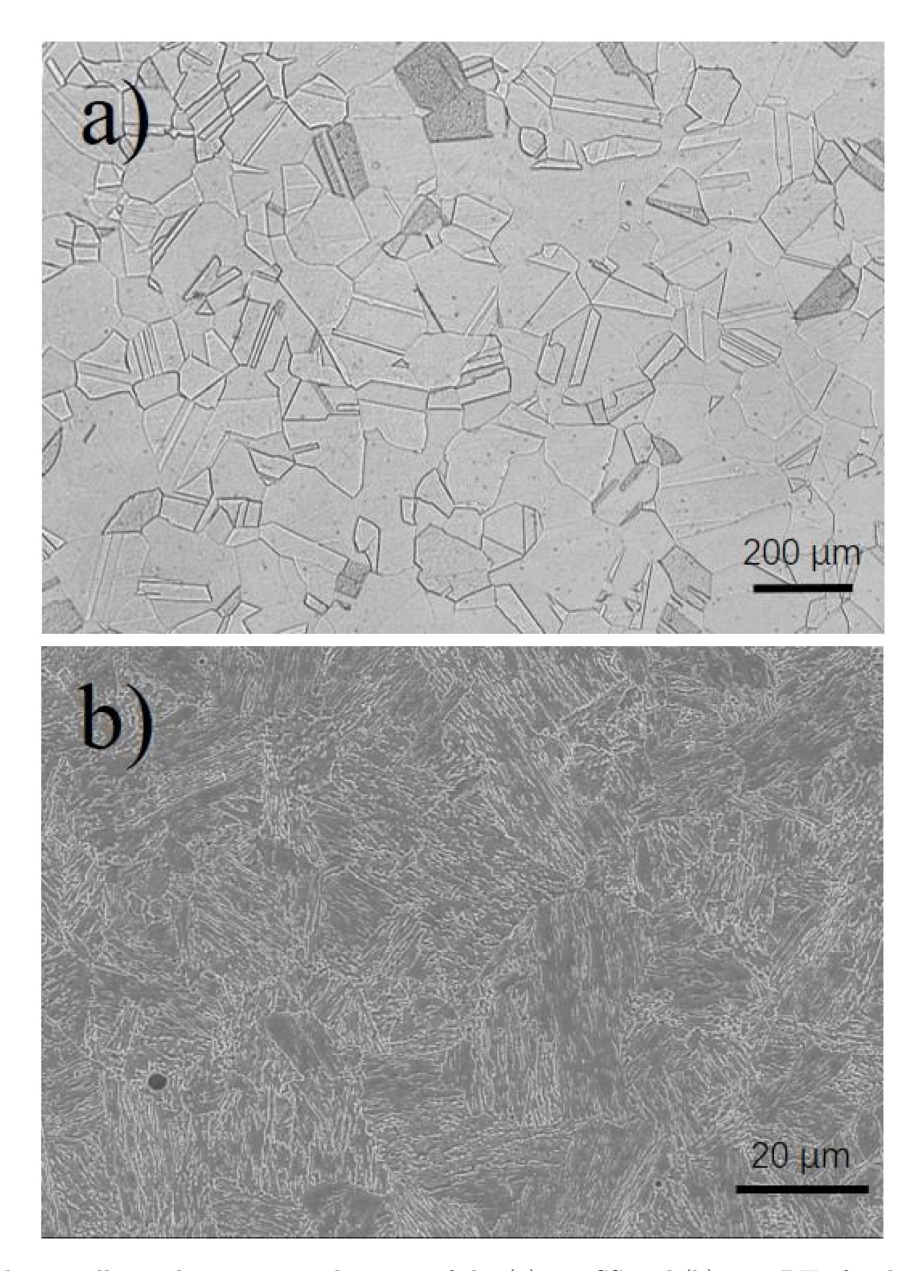


Figure 12: The metallographic micrograph image of the (a) 304 SS and (b) 17-4 PH after heat treatment. 304 SS shows a typical morphology of austenitic steel, while 17-4 PH shows a martensitic structure and round inclusion can be occasionally observed on its surface[41].

Another cutting-edge approach is to isolate single pit events and monitor them acoustically. Wu et al. performed experiments where only one pit was allowed to form on these specimen with the help of micro-electrodes[41]. In the study they compared the AE from a single pit on 304 SS versus on 17-4PH stainless. These two materials have austenitic structure and martensitic structure respectively, as illustrated in Figure 12. Interestingly, the single pit on 17-4PH was much more acoustically active than that on 304 ss, producing dozens of AE signals, whereas the pit of 304 ss emitted very few[41]. In other words, the pit of martensitic stainless steel triggered a lot of AE signals because of intense local reactions (possibly due to hydrogen bubble formation and rupture inside the pit). Comparatively, austenitic 304 stainless steel exhibited a more stable passive film and less aggressive pit chemistry, resulting in reduced acoustic activity[41]. This study demonstrated how material and environmental factors such as alloy composition, can influence the acoustic signature of pitting. It also reinforced the role of hydrogen bubble dynamics in generating AE. By using high-speed camera observations, the authors confirmed that bubbles forming and perturbing the electrolyte inside the pit coincided with AE bursts.

Meanwhile, given the complexity of AE data from corrosion, recent studies increasingly employ statistical and machine learning techniques to interpret the signals. Cluster analysis, for example, has been used to categorize AE hits into groups corresponding to different physical mechanisms. Bi et al. applied

K-means clustering to AE signals from pitting of low carbon steel in combination with electrochemical measurements. And they successfully separated signals into clusters attributed to hydrogen bubble activity, oxide film rupture, and stable pit growth[62]. Such clustering approaches, often based on features such as amplitude, duration, frequency and counts, help filter out noise and assign a likely reason to each AE event. Similarly, researchers have explored supervised learning to classify AE signals of 304 stainless during corrosion, and this improved the reliability of pitting detection by recognizing the typical waveform patterns of corrosion-related AE versus unrelated noise[63]. These analysis techniques represent the state-of-the-art in processing AE data, turning large volumes of raw acoustic hits into meaningful information about corrosion processes.

Another significant trend in current research is translating these techniques to field or industrial scenarios. For example, installing AE sensors on pipelines, storage tanks, or infrastructure to monitor for corrosion is increasingly considered in structural health monitoring programs. One challenge is that traditional AE sensors require direct contact with the metal surface, which might not be feasible if the surface is covered (by insulation, coatings, marine growth, etc.). To overcome this, non-contact AE techniques are being developed. Alkhateeb et al. demonstrated a non-contact AE monitoring system for corrosion under marine biofouling[64]. They used sensitive air-coupled ultrasonic sensors placed at a fixed distance from a steel specimen immersed in seawater. Despite a 12 dB attenuation of the acoustic signal due to the soft marine growth layer, the system still achieved a satisfactory signal-to-noise ratio and could detect corrosion-related AE events[64]. They even implemented source localization algorithms to triangulate the position of corrosion events on the remote structure[64]. This kind of research is pushing AE towards practical monitoring of real structures where pitting might occur in inaccessible areas.

3 Research objectives

3.1 Knowledge gaps

Many studies have reported that transient acoustic emission (AE) signals accompany the initiation and growth of corrosion pits in metals. However, the precise physical origin of these pitting-induced AE events remains ambiguous and under active debate. It is not yet clear whether the AE bursts arise directly from the electrochemical reactions of pitting or from secondary physical processes occurring during pit development. For example, some researchers attribute the detected AE during pitting to the formation and violent rupture of hydrogen bubbles within the pit (and the associated disturbances in the local electrolyte). In contrast, other studies propose that the AE signatures are generated by mechanical disruptions such as the breakdown of the passive oxide film or the disintegration of pit cap. This conflicting evidence shows a significant gap in the literature: While AE activity is clearly correlated with pitting corrosion, its exact source mechanism, chemical vs. mechanical, has not yet been conclusively identified.

3.2 Research questions

Main research question: What is the casual relationship between acoustic signals and electrochemical reactions (e.g. metal dissolution) or secondary phenomenon (e.g., passivation film rupture or hydrogen bubble?

Subquestion (i): How can the acoustic emission signals of passive film breakdown or bubbling during pitting corrosion be distinguished from other corrosion events?

Subquestion (ii): What are the defining AE parameters (e.g., amplitude, duration, frequency) that help to distinguish AE signals arising from passive film rupture or hydrogen bubbles?

3.3 Novelty

This combination introduces a multi-modal methodology by combining acoustic emission and electrochemical noise to investigate pitting corrosion in stainless steel, which is a significant advancement beyond the studies with a single technique. Previously, AE monitoring has been applied to detect pit initiation and propagation in stainless steel, but interpreting the source of AE signals has remained challenging. These signals can arise either from the electrochemical pit growth process or from secondary mechanical events such as hydrogen bubble activation and passive film rupture. This leads to ambiguity in their origin. EN measurements could capture characteristic transient fluctuations in current/potential that indicate metastable or stable pitting events. Meanwhile, with the help of optical microscopy, we can see if hydrogen bubbles occur. In this planned research, both techniques are integrated simultaneously, and this enables to see the correlation of acoustic data and electrochemical data. This novel approach allows us to distinguish the ambiguous AE signatures by confirming whether a given acoustic burst is linked to an electrochemical reaction or to a mechanical disturbance such as bubble bursting or film breakage during corrosion.

4 Methodology

4.1 Potential combinations of AE and Electrochemical techniques

Based on the literature review, in pitting corrosion studies, acoustic emission monitoring can be paired with various potential electrochemical techniques to provide complementary insights. Below is an overview of each combination.

4.1.1 AE + Potentiodynamic Polarization (PDP)

Potentiodynamic polarization involves sweeping the electrode potential at a controlled rate to induce and examine corrosion reactions. In the context of pitting, PDP is used to determine characteristic potentials such as the pitting potential (Ep) and the repassivation potential (Erep). When combined with AE monitoring, this technique provides a controlled way to provoke pit formation while "listening" for the acoustic signals generated by pit nucleation and growth. For example, as the potential is anodically scanned through the passive region into the pitting regime, a sudden increase in current (indicating passivity breakdown) often coincides with detectable AE bursts. Thus, the AE+PDP combination allows identification of the potential at which pitting initiates and links it to acoustic signatures of that event. This is useful for quantifying stainless steel's pitting resistance (via Epit) while simultaneously capturing the mechanistic indication of pit onset. It should be noted that PDP is an accelerated test. By driving the electrode to increasingly aggressive conditions, it forces pit initiation, which could reduce the time of experiment. But this may produce clear AE signals and perturb the natural corrosion process significantly.

4.1.2 AE + Electrochemical Impedance Spectroscopy (EIS)

Electrochemical impedance spectroscopy is a frequency-domain technique in which a small AC voltage perturbation is applied to the metal, and the resulting current response is measured over a range of frequencies. When AE monitoring is integrated with EIS, the goal is to correlate specific impedance changes with acoustic events. For example, an impedance decrease or new time-constant signaling pit initiation might coincide with an AE burst indicating film rupture or pit growth. In practice, an AE+EIS setup involves pausing at intervals to record an impedance spectrum while continuously listening for AE hits. The strength of AE+EIS lies in its ability to confirm the presence and development of pits through changes in electrical response while capturing the real-time physical events. However, EIS is inherently a slow measurement. It excels in measuring overall corrosion progression and film breakdown but it is less direct in capturing the exact moment of a single pit event, since impedance data are in frequency. This trade-off will be discussed further in the comparative evaluation.

4.1.3 AE + Electrochemical Noise (EN)

EN monitoring is a passive technique: unlike PDP or even EIS, no external stimulus is applied to the system; instead, the corrosion process generates its own 'signal'. This makes EN extremely suitable for detecting early pitting events. Combining AE with EN creates a powerful in-situ monitoring system in which two independent channels track the corrosion in real-time. The AE sensor detects the acoustic signals from events like film rupture, crack formation, or gas bubble collapse, while the EN measurement detects the electrochemical signatures of these same events. The two datasets are acquired simultaneously and can be time synchronized. In practice, an AE+EN experiment on stainless steel pitting might be conducted under open-circuit conditions in a chloride solution with low pH. When a significant transient occurs, one would expect concurrent indications: e.g. a sharp current noise peak accompanied by an AE burst. Such coincidences strongly indicate a pitting event.

4.2 Comparative Evaluation of AE and Electrochemical Combinations

To determine the most suitable experimental approach for this research, the three AE-electrochemical combinations are compared across several key criteria: (i) sensitivity to early corrosion events, (ii) ability to distinguish signal sources, (iii) degree of perturbation to the system, (iv) temporal resolution, and (v) feasibility for long-term monitoring, as well as practical considerations such as data interpretation complexity, signal overlap, and drift. The following comparative analysis highlights the strengths and limitations of each combination and leads to the rationale for selecting the AE+EN method for this thesis.

4.2.1 Sensitivity to Early Corrosion Events

An effective monitoring technique should detect the very onset of pitting corrosion, the moment when a pit nucleus forms or a passive film first breaks down. Among the three combinations, AE+EN provides the highest sensitivity to these incipient events. Because EN captures small fluctuations in current or potential and it can reveal metastable pitting events that produce only tiny amounts of dissolution. These events might be undetectable by slower or less sensitive methods. Studies have shown that using AE and EN together enables detection of characteristic burst signals and transient electrochemical spikes associated with pit initiation well before the damage is macroscopically visible [65], [66]. In contrast, AE+PDP is less sensitive to the earliest events because the potentiodynamic scan tends to cover very small corrosion fluctuations. As the current is rising, minor transients might be lost in the background. Nevertheless, AE+PDP is quite adept at pinpointing the onset of stable pitting. As soon as the polarization potential reaches the breakdown threshold, a clear surge in current occurs and typically a flurry of AE activity is observed[9],[60]. For AE+EIS, it is the least sensitive to an individual early pit event. EIS excels in revealing that some degradation has occurred. It does so by averaging the response over time and frequency, which means it cannot detect a single tiny pit in real-time. One might perform EIS after a short exposure to see if the resistance of the passive film has decreased, which would imply that pits have formed. So this is a retrospective detection rather than a real-time method.

4.2.2 Ability to Distinguish Signal Sources

AE+EN offers a particularly powerful advantage: By simultaneously observing electrochemical noise, it becomes possible to tell whether an acoustic event was accompanied by electrochemical activity. By correlating AE and EN in time, one can thus infer the nature of the event. For AE+PDP, the polarization potential at which an AE event occurs gives clues to its origin. For instance, during a potentiodynamic scan, AE activity that erupts precisely at the pitting potential is likely due to pit initiation because that is when the passive film is breaking down. If acoustic events are recorded at more positive potentials above Epit, they might correspond to cracking as pits grow larger or mechanical fracturing of cover deposits. If they occur at potentials below Epit in the cathodic range, they might be due to hydrogen evolution processes. Thus, the potential context in AE+PDP experiments can help distinguish signals. However, PDP's ability to separate sources is still limited – many processes overlap around the pitting potential, and all contribute to the current increase, so additional clues are needed to be certain. AE+EIS is the least direct in differentiating AE signal sources. Because EIS yields information about the overall state of the surface rather than time specific events, it cannot indicate which acoustic signal corresponds to which process in real-time. At best, people could use EIS results to infer what processes are generally occurring. If an AE signal is recorded and subsequently EIS shows a new pit-induced feature, one might surmise that the prior AE was related to pit growth. But this is indirect and not time-synchronized.

4.2.3 Perturbation of the System and Long-Term Feasibility

For AE+PDP, it is inherently a strong perturbation. The technique forces the metal to corrode by driving the potential, often far beyond the open-circuit potential in order to trigger pits. This provides valuable data on pit susceptibility, but it does not reflect a freely corroding system. Because PDP actively accelerates corrosion, it is typically a short-term test. One cannot continuously scan a specimen over hours or days without effectively destroying the sample or significantly altering its surface conditions. Thus, AE+PDP is usually employed in a one-off manner to identify when and how pits initiate, rather than to passively observe corrosion over time. AE+EIS is a gentler perturbation: it uses a small AC signal that generally does not disturb the corrosion process in more than a minimal way. In many cases, a properly small excitation in EIS is considered non-destructive and will not initiate corrosion that wouldn't occur otherwise. However, each EIS measurement takes time from minutes to tens of minutes for a full spectrum. If significant corrosion changes occur during the impedance scan, the data quality will be influenced. For long-term monitoring, one could perform EIS at intervals to track the evolution of the corrosion state, but this makes it more complicated when combined to AE. Hence for long-term observation it is in a stepwise fashion, but not truly continuous and could potentially disturb delicate processes if not carefully controlled. In contrast, AE+EN is entirely non-intrusive and appropriate to longterm, real-time monitoring. Both AE and EN are passive techniques, so the sample can be left at opencircuit potential, and neither the acoustic sensor nor the noise measuring device significantly perturbs the reaction. As Hladky and Dawson's seminal work noted, unlike conventional electrochemical methods that impose external perturbations, EN simply listens to the 'natural' fluctuations of corrosion [56]. Similarly, the AE transducer only detects elastic waves and does not inject energy into the sample. This means the corrosion process can proceed unaltered for hours or days while data are being collected. AE+EN can monitor pitting corrosion over very long durations and it is limited only by instrumentation and storage. To sum up, with respect to system perturbation and long-term usage, AE+EN is the most favorable combination. It is non destructive and can operate long, this makes it ideal for monitoring of corrosion processes over time. AE+EIS is moderate with low perturbation, but not truly continuous in time. AE+PDP is highly perturbative and only suitable for short, forced tests.

4.3 Signal processing

4.3.1 AE signal processing

An amplitude–time plot was generated to characterize the overall distribution of AE signals. Cumulative hit counts were plotted to characterize the speed of generation of AE signals. Peak-frequency probability densities were estimated in three amplitude bins (¡40 dB, 40–60 dB, ¿60 dB) to compare spectral tendencies. Duration vs. peak frequency and duration vs. time were constructed to track changes in time scales. For comparability, the test was divided into two windows (0–17 h and 17–39 h). The b-value plot was generated to quantify the time-resolved evolution of AE activity.

4.3.2 En signal processing

Pre-processing

As Open Circuit Potential (OCP) often drifts, a trend removal step is required to isolate the stochastic component of interest, which is known as detrending. Polynomial/moving-average detrending, time-frequency detrending, and related approaches have been evaluated systematically [67]. In practice, subtracting a slowly varying baseline implements an effective high-pass filter whose corner frequency is governed by the baseline window/degree.

Time-domain analysis

Global intensity (RMS and standard deviation)

After detrending, the overall noise level is usually summarized by the root-mean-square (RMS) or the standard deviation (STD). These second order statistics quantify fluctuation strength and often increase with corrosion activity. They are among the sequence-independent parameters recommended by Cottis for baseline characterization [68].

Local activity (rolling standard deviation)

To localize activity in time, a moving (rolling) STD is computed over a sliding window. Peaks in the rolling STD define active episodes of enhanced fluctuation energy and are frequently used as markers for passive-film breakdown or repassivation phases before finer transient analysis. This reflects the general recommendation to complement global descriptors with windowed statistics when mechanisms evolve during the test [68].

The Z-score is a normalized, dimensionless metric used in time-domain analysis to identify anomalous fluctuations in electrochemical noise signals. For each time sample x_i , the Z-score is computed by

$$Z_i = \frac{x_i - \mu}{\sigma} \tag{11}$$

where μ and σ are the mean and standard deviation of the detrended noise time series, respectively. A large absolute Z-score (for example $|Z_i| > 3$ or $|Z_i| > 4$) denotes a rare, high-amplitude transient event, which may correspond to phenomena such as passive-film breakage, metastable pit nucleation or hydrogen bubble detachment. This normalization facilitates event detection that is robust across different baseline noise levels. In this work, the Z-score method was introduced as an extension of conventional time-domain statistical analysis to enhance the detection of spikes and transient events in electrochemical noise signals. It has similar mathematical principles with other descriptors of transient activity [69], [70].

Frequency-domain analysis

After removal of the slow baseline drift (via detrending or high-pass filtering), the power spectral density (PSD) of the residual potential or current noise is estimated using methods such as Welch's averaged periodogram or standard periodogram/FFT techniques. Welch's method divides the signal into overlapping segments, applies windowing (e.g., Hanning or Hamming windows), averages the periodograms to reduce variance, and yields a smoother spectral estimate[71]. In contrast, the basic periodogram may suffer from spectral leakage and high variance unless long signals and proper windowing are used[72]. Once the PSD is obtained, the dominant frequency (i.e., the frequency at which the spectral power reaches

its maximum, excluding the DC or near-zero-frequency component) is identified; this frequency often correlates with specific processes such as passive-film rupture or gas bubble release [68], [69].

To sum up, in this study the electrochemical noise data were processed as below: The algorithm first removed slow baseline drift by linear detrending and 10 s moving-average filtering, isolating the stochastic potential noise. Time-domain parameters, including standard deviation and root-mean-square (RMS), were computed to quantify global fluctuation intensity, while a one-minute rolling standard deviation localized transient bursts indicative of passive-film breakdown or repassivation. A Z-score transformation provided a normalized measure of rare high-amplitude spikes. Frequency-domain characteristics were then derived by estimating the power spectral density using Welch method, determining the dominant frequency and integrating spectral power over low $(0.001-0.1~{\rm Hz})$, mid $(0.1-1~{\rm Hz})$, and high $(1-10~{\rm Hz})$ bands. Automated event detection identified passivation-breakdown episodes when the rolling standard deviation exceeded three standard deviations for at least five seconds and clustered Z-score spikes $(Z>4, > 1~{\rm mV})$ as hydrogen-bubble events. These results were generated to provide a quantitative link between electrochemical noise signatures and the underlying pitting corrosion processes.

5 Experimental

5.1 Materials and solution

The test specimens are AISI 304 stainless steel rods, purchased from Evek GmbH (Germany), with a length of 50 cm and a diameter of 1 cm. For samples of this size, preliminary experiments have confirmed that reflections of AE signals do not significantly affect the results. Additionally, the cross-section of rod-shape stainless steel bars is more susceptible to pitting corrosion. Detailed composition about the specimen is shown in Table 1. Upon receipt, the metal samples were sequentially polished using silicon carbide papers of grit sizes 80, 200, 600, 800, 1200, and 2000, followed by rinsing with deionized water to remove any surface contaminants. The specimens will be immersed in a 3.5 wt% NaCl solution, with the pH adjusted to 2 using hydrochloric acid to promote aggressive localized corrosion. Hydrochloric acid was selected over sulfuric acid due to its ability to elevate chloride ion concentration, which is a critical factor in promoting the initiation and propagation of pitting corrosion. All experiments will be conducted under open-circuit potential conditions for a duration of three days.

Table 1: Chemical composition of the sample (wt.%)

C (wt.%)	Si (wt.%)	Mn (wt.%)	P (wt.%)	S (wt.%)	Cr (wt.%)	Ni (wt.%)	N (wt.%)
≤ 0.07	≤ 1	≤ 2	≤ 0.045	≤ 0.015	17.5 – 19.5	8 - 10.5	0.11

5.2 AE experimental setup and parameter

Acoustic emission (AE) signals generated during the pitting corrosion process were continuously monitored using a fully digital AE data acquisition system (AMSY-6, Vallen Systeme GmbH, Germany). The AE sensor employed was an R15 α resonant-type sensor with a peak sensitivity around 150 kHz, suitable for capturing high-frequency emission events associated with localized corrosion phenomena. Parafilm was used as an insulating layer between the metal rod specimen and the mounting fixture to prevent any interference from the fixture with the AE signals. The AE sensor was secured using a 3D-printed holder designed to match the sensor's geometry. To eliminate environmental and background noise, a band-pass filter with a frequency range of 40–180 kHz was applied at the front end. The threshold for signal detection was set at 19.2 dB to ensure reliable acquisition of relevant AE events while minimizing spurious triggers. The AE signals were sampled at a rate of 10 MHz, providing high temporal resolution. The system was configured with a rearm time of 100 μ s and a duration discrimination time of 100 μ s to avoid counting overlapping signals or low-energy noise bursts as valid events. A pre-trigger time of 160 μ s and a post-duration window of 160 μ s were set to capture the complete waveform surrounding each AE hit. Signal amplification was performed using an AEP5 preamplifier with a fixed gain of +40 dB, ensuring adequate signal strength for analysis without introducing distortion.

5.3 EN experimental setup and parameter

Electrochemical noise (EN) measurements were conducted to investigate the corrosion behavior of AISI 304 stainless steel under open-circuit conditions. A conventional two-electrode electrochemical cell was employed, consisting of the AISI 304 specimen as the working electrode and a saturated Ag/AgCl electrode serving as the reference. Both electrodes were thoroughly cleaned with deionized water before use to minimize contamination and ensure signal fidelity. The electrodes were connected to a potentiostat configured for EN acquisition. The data acquisition was conducted with a sampling interval of 0.05 s, corresponding to a sampling frequency of 20 Hz. The current range was set to 100 mA and the potential range to $\pm 400 \text{ mV}$. A 10 Hz low-pass filter was applied to suppress high-frequency noise, and the system operated under a "high stability" mode to ensure data reliability.

5.4 Complete experimental setup

To investigate the acoustic emission and electrochemical noise responses during pitting corrosion of stainless steel, a combined in-situ monitoring system was established. Figure 13 illustrates the schematic experimental setup. Figure 14 shows the experimental setup in practice.

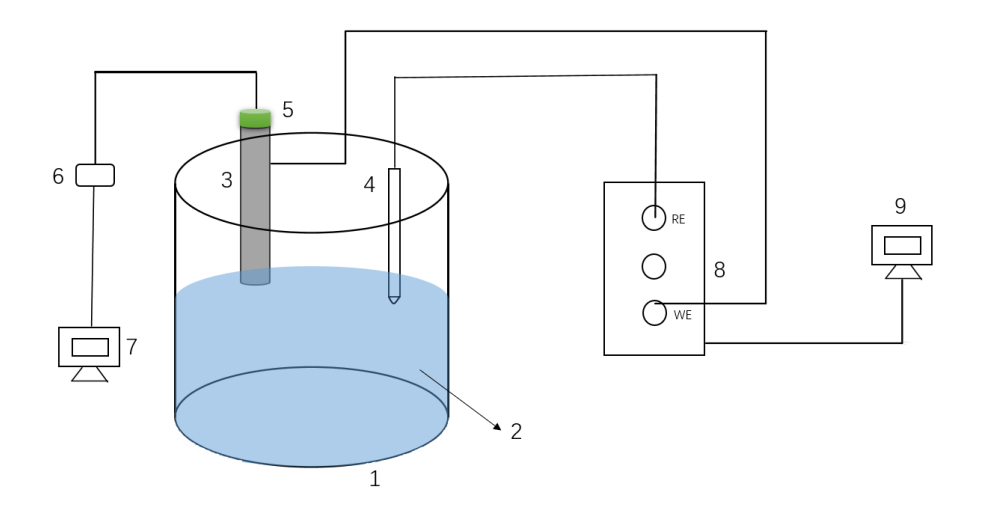


Figure 13: Schematic diagram of the experimental setup (1:Corossion cell, 2: 3.5 wt%NaCl solotion (pH=2), 3: 304 stainless steel rod, 4: Ag/AgCl electrode, 5: AE sensor, 6: Preamplifier, 7: AE data acquisition computer, 8: Electrochemical workstation, 9: EN data acquisition computer



Figure 14: Experimental setup in practice

6 Results and discussion

6.1 Photos of experimental setup after experiment

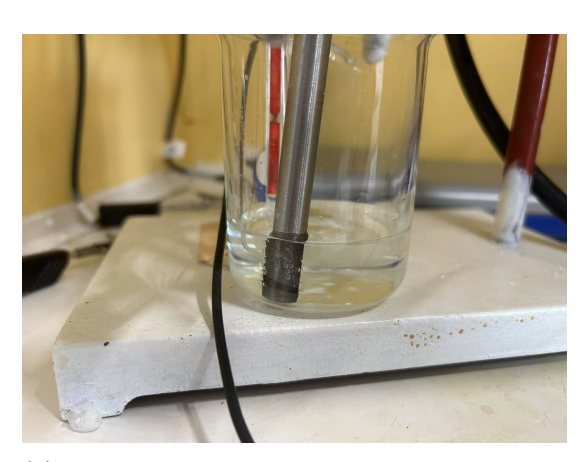
By comparing the setup images taken before and after the experiment, it was noted that the vertical position of the metal rod specimen decreased by approximately 2 centimeters upon completion of the test, as shown in Figure 15. This displacement is likely attributed to the relatively high weight of the specimen, which may have caused insufficient clamping force by the fixture.

The downward movement of the sample would have involved frictional contact with the metallic clamp, potentially generating unintended acoustic emission (AE) signals. To ensure the reliability of the experimental data, it is essential to accurately determine both the time of occurrence and the duration of this slippage event. A more detailed analysis of this incident will be presented in the following section discussing AE results.

It was also observed that in the later stages of the experiment, a large number of gas bubbles were observed at the surface of the immersed metal rod specimen. These bubbles were likely formed by the continuous accumulation of hydrogen generated during the corrosion process. Such hydrogen bubbles are considered potential sources of acoustic emission (AE) signals.



(a) Experimental setup



(b) Experimental setup after experiment, showing the offset of the AISI304 bar.

Figure 15: Experimental setup before and after experiment

6.2 Optical Microscopy

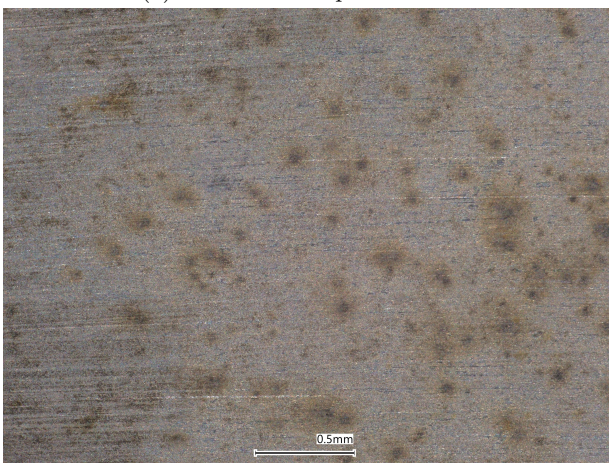
Figure 16 shows the surface morphology of a 304 stainless steel specimen after 3 days of immersion in a 3.5 wt% NaCl solution (pH = 2). Figure 16a presents a low-magnification ($20\times$) overview of the entire specimen surface, while Figure 16b shows a locally magnified view at $80\times$. As expected, corrosion traces are mainly concentrated in the central region, forming large areas of densely distributed dark brown corrosion products. The peripheral regions appear relatively clean, this suggests a pronounced central aggregation tendency during corrosion. The surface still exhibits faint polishing marks that are not fully covered by corrosion products, indicating that the corrosion process exhibits strong localization.

Figure 17 shows the microscopy image of the AISI 304 stainless steel specimen after the test in a 3.5 wt% NaCl solution (pH = 2), captured at $500 \times$ magnification. The scale bar indicates 100 µm. Several irregularly distributed dark spots can be observed on the surface, ranging from approximately 20–80 µm in diameter. These darkened areas are indicative of localized corrosion product accumulation and pitting because they exhibit typical features of pitting corrosion morphology.

Noticeable surface grinding marks remain visible, this suggests that corrosion was localised. However, the overall surface morphology also indicates that uniform corrosion is simultaneously present. The fuzzy edges of the pits imply that they may be partially covered by corrosion products such as metal chlorides or hydrolyzed species formed during pit propagation.



(a) OM corrosion product X20



(b) OM corrosion product X80

Figure 16: OM corrosion product

Considering the aggressive chloride-rich and acidic environment, this morphology can be attributed to chloride-induced pitting corrosion. The following is possible mechanisms:

- Local breakdown of the passive film;
- Anodic metal dissolution (Fe \rightarrow Fe²⁺ + 2e⁻) within the pit;
- Migration and accumulation of chloride ions, causing local acidification (Fe²⁺ + H₂O \rightarrow FeOH⁺ + H⁺);
- Hydrogen gas evolution, which may contribute to surface disturbance and acoustic signal generation $(2H^+ + 2e^- \rightarrow H_2 \uparrow)$.

In summary, these surface images provides direct morphological evidence of pitting. And they could support the presence of highly localized electrochemical and mechanical events. These are potentially linked to AE sources such as hydrogen bubble formation and rupture or passive film breakdown, which will be further discussed in the following chapters.

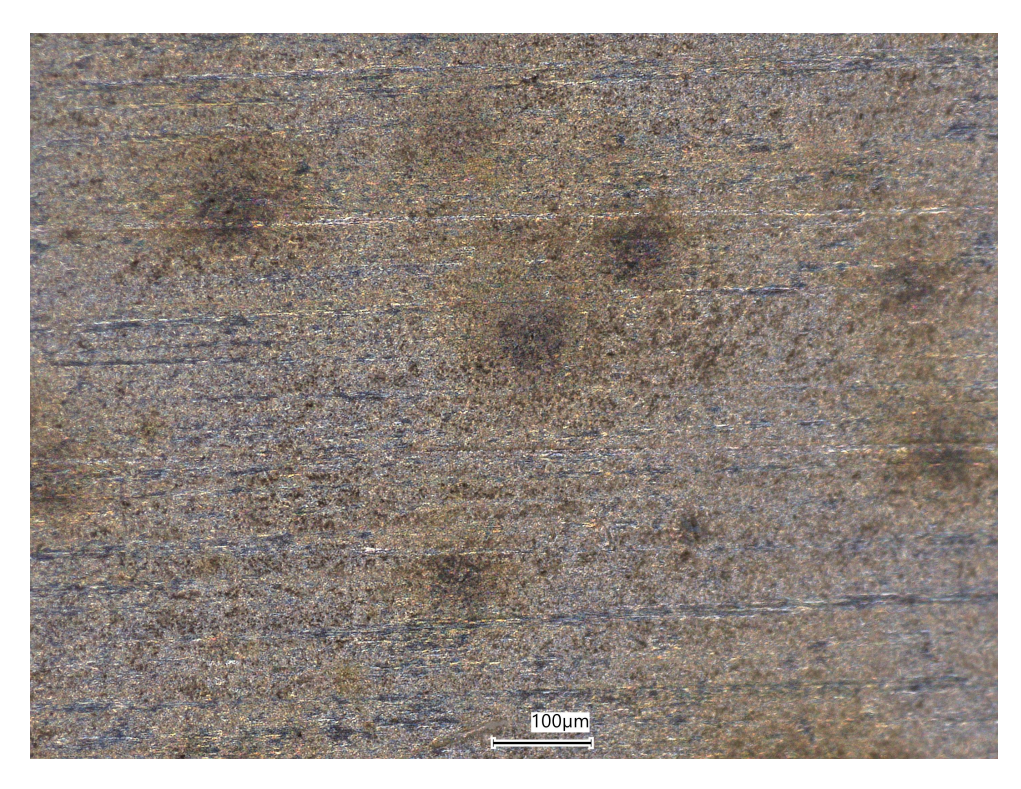


Figure 17: detailed corrosion morphology

6.3 AE results

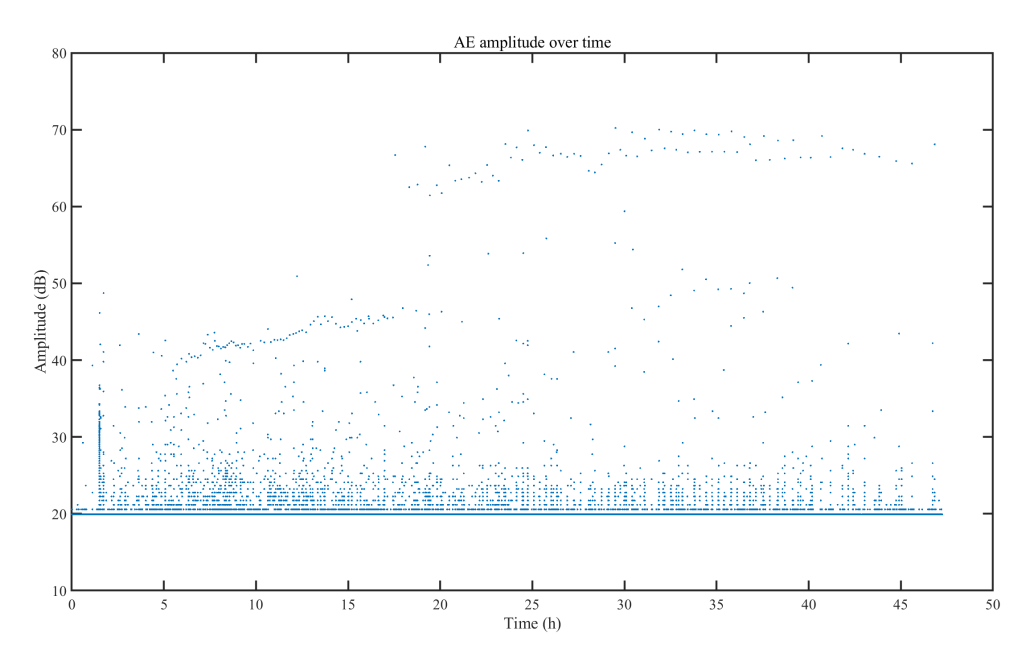


Figure 18: AE signal amplitude distribution over time

Figure 18 shows the distribution of acoustic emission (AE) signal amplitudes over time, expressed in decibels (dB). The x-axis shows the time since start, and the y-axis indicates the amplitude range, spanning from approximately 20 dB to 75 dB. In the beginning there was almost no AE signals and this lasts for about an hour. This initial period involved system stabilization after immersion. And this indicated negligible corrosion activit. After about an hour a number of AE signals were detected. During this stage this could due to chloride ions continuously attacking the passive film. And that triggered localized film breakdown and intermittent repassivation. AE signals became more frequent, with the majority of amplitudes ranging from 40 to 50 dB. From approximately the 16th hour on, a shift in AE

behavior was observed. AE signal amplitudes increased significantly, with many signals in the 60-70 dB range. In the same time, the number of AE signals in the 40-50 dB range dropped markedly compared to the previous stage. This reduction in AE activity within the 40-50 dB range may due to the formation of new pits had significantly decreased. It may suggest that the corrosion process had progressed into a more stable phase, characterized by the continued growth and development of previously initiated pits, rather than the nucleation of new ones.

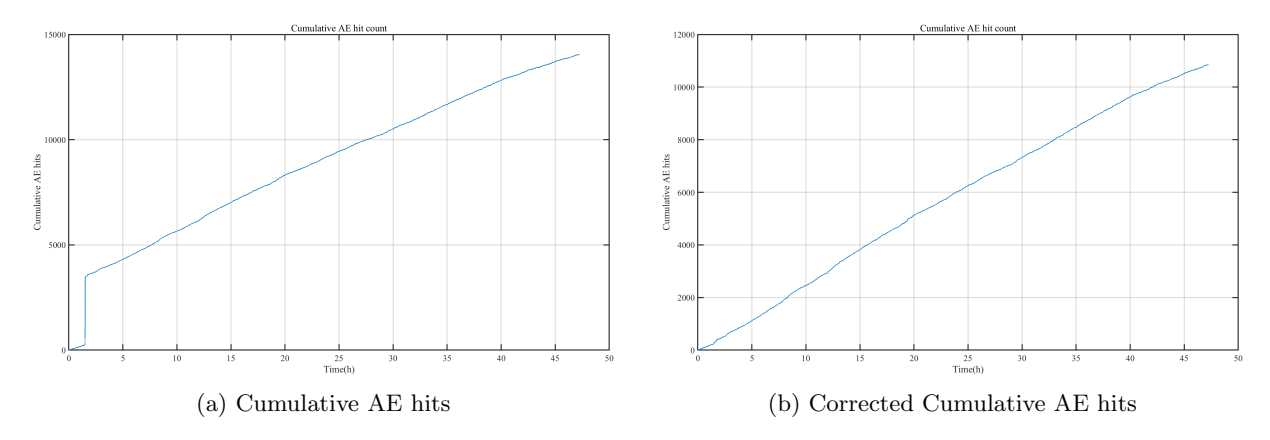


Figure 19: Cumulative AE hit count

Figure 19a presents the cumulative AE hit count as a function of time throughout the experiment. The overall trend of the curve demonstrates a steady and nearly linear increase in cumulative AE hits, with only minor local variations in slope. This observation indicates that the rate of AE event generation remained relatively constant during the entire immersion period. Given that the experiment was conducted under free corrosion conditions without externally applied potential, the AE signals primarily originated from spontaneous localized events such as passive film breakdown and hydrogen bubble evolution. While these transient events are acoustically significant, often producing higher amplitude bursts. But they are in minority.

In contrast, the majority of AE activity is likely attributed to low-amplitude background signals (around 20 dB). These low amplitude events dominate the cumulative count and result in a stable overall growth rate of AE hits. Therefore, according to Figure 18 and Figure 19a, the steady slope of the cumulative curve reflects a persistent but low intensity corrosion process with occasional higher impact events superimposed. Notably, as shown in Figure 19a, a burst of AE activity occurred between 5399 and 5435 seconds after the start of the experiment. During this period, the slope of the cumulative AE hit curve became nearly vertical, indicating a large number of AE signals in a short time. This stage lasted for approximately 36 seconds. In Figure 18, a cluster of unusually high amplitude signals was also observed. And their timestamps match. This confirms that both AE plots reflect the same sudden event. Combined with previous observations that the metal rod slipped downward during the test, it can be inferred that this slippage occurred at this time. The movement likely caused friction with the fixture, resulting in a short but intense AE signal burst. This mechanical disturbance should be considered separately from corrosion-related AE activity in the analysis. Figure 19b shows the corrected cumulative AE hit count. By removing the signals during this thirty seconds the AE signals from the slippage of the sample rod was removed.

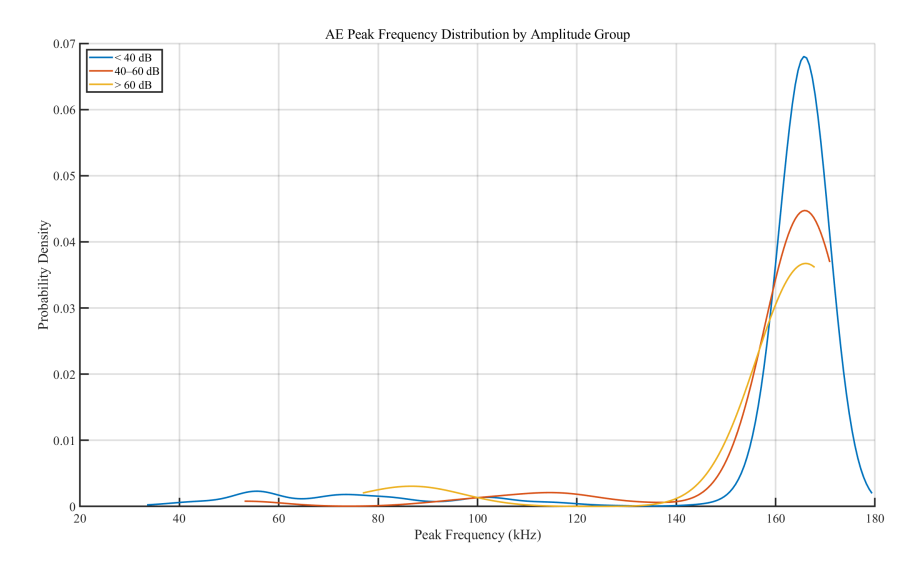


Figure 20: AE Peak Frequency Distribution by Amplitude Group

Figure 20 illustrates the distribution of acoustic emission peak frequencies for different amplitude ranges (<40 dB, 40–60 dB, >60 dB). These ranges are usually considered as low amplitude, medium amplitude and high amplitude [73], [74]. The horizontal axis represents the peak frequency (kHz), while the vertical axis denotes the probability density, indicating the relative probability of signals occurring within specific frequency ranges. The distribution curves of all amplitude ranges exhibit a pronounced peak in the high-frequency region, with the <40 dB group showing the sharpest peak and the high-st probability density. The spectrum of the medium-amplitude group is slightly broader, while the high-amplitude group displays the widest distribution. In the lower-frequency region, small fluctuations can be observed for all amplitude groups (e.g., around 60 kHz, 80–100 kHz, and 120 kHz), but their probability densities remain significantly lower than that of the dominant high-frequency peak.

In acidic chloride media, the nucleation, growth, and rupture of hydrogen bubbles inside pits is one of the most frequently identified AE sources during corrosion. Numerous studies report bubble-related AE with dominant frequency bands around 100–300 kHz, with peaks near 150–200 kHz being common. Likewise, in pitting or potentiostatic experiments on 304 stainless steel, the resonance-type signals observed during the propagation stage have repeatedly been associated with bubble activity[73]. This agrees with the peak frequency value observed in Figure 20. At the same time, micro-crack type acoustic signals are also commonly found in the 100–200 kHz band. In this experiment there is no external loading, so such events are usually infrequent. However, as corrosion progresses, the development of local stresses or the rupture of pit covers can contribute additional energy in the 150–200 kHz range. The optical pictures shows a lot of pits and the presence of corrosion caps. This indicates that the high-frequency AE near 160 kHz also may include contributions from local stress accumulation and pit-cover rupture[3],[75]. Those small fluctuations between 40 and 120 kHz range may correspond to secondary sources with relatively low natural frequencies. These fluctuations may include frictional interactions between corrosion debris and pit walls, or partial collapse of the corrosion-product layer.

However, it should be emphasized that the peak near 160 kHz observed in the present study cannot be attributed solely to the intrinsic characteristics of the corrosion-induced acoustic sources. The R15 α sensor employed in this work is a narrowband resonant sensor, with a specified operating range of 50–400 kHz and a maximum sensitivity near its resonant frequency of approximately 150 kHz. Detailed information about R15 α is given in the attachment. Consequently, the sensor itself acts as a frequency-selective filter, preferentially amplifying signals in this band while attenuating contributions outside its resonance. Similar phenomenon was reported in some studies[76]. As a result, AE events originating from diverse physical processes (e.g., hydrogen bubble formation and rupture, passive film breakdown, pit cover collapse, or detachment of corrosion products) may all be projected into the 150–170 kHz region due to the resonance response of the sensor. This instrumental effect explains why the dominant frequency remains remarkably stable across amplitude classes in the present dataset.

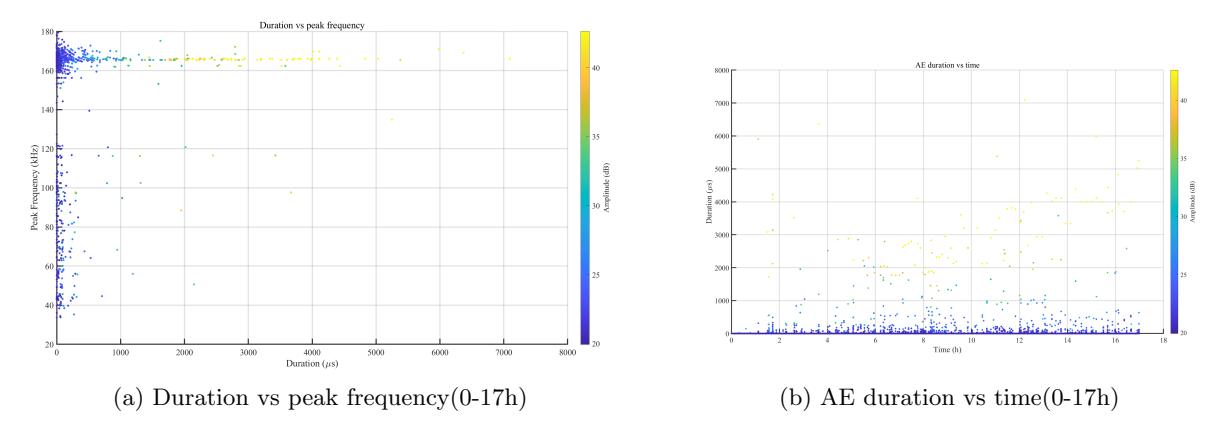


Figure 21: AE duration vs time and Duration vs peak frequency(0-17h)

Figure 21 shows AE duration vs time and Duration vs peak frequency. In Figure 21a, most events have their peak frequency tightly clustered around 165–172 kHz. As noted for t=2-17h, such a bundle typically reflects the narrow-band resonance of the sensor rather than genuine changes in the source mechanism. This agrees with Figure 20. Considering narrow-band AE sensors are known to pull peak frequency toward their resonance, therefore PF-based mechanism discrimination is limited in such setups. Nevertheless, we may still obtain some information from it. A small number of low-frequency points (40–120 kHz) occur mainly in short-duration events. This suggests weaker sources such as breakdown of passive film exist. And it could be seen that the long-duration events (2–3 ms) still lie primarily near 170 kHz. This indicates that the increase in duration time is predominantly a time-domain effect. For example, event overlap, trailing or ring-down rather than a downward shift of the source frequency. Figure 21b indicates that short-duration events (less than 200 μs) occur throughout 0-17 h, but the upper peak value of duration clearly rises after around 12 h, with numerous long events (1-5 ms) that also show higher amplitude. This indicates activities become more sustained and energetic.

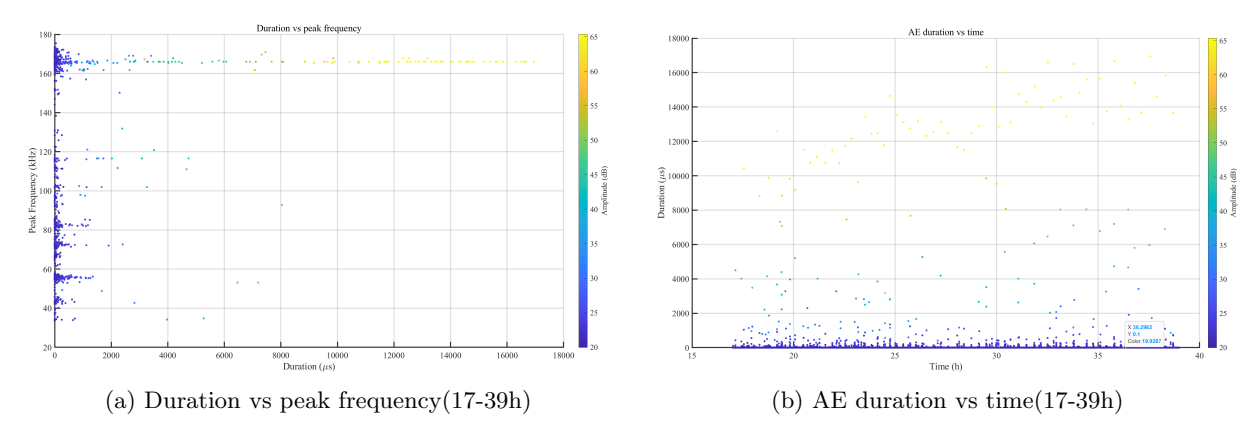


Figure 22: AE duration vs time and Duration vs peak frequency(17-39h)

Figure 22 shows the Duration vs peak frequency and AE duration vs time for t=17-39h. In Figure 22a, peak frequency still remains tightly clustered near 170 kHz across the entire duration range due to the sensor effect. So limited information can be obtained. In figure 22b, from 20h onward, especially after 30h, the duration of events becomes even longer, with maximum value of approximately 17ms. These long events are systematically higher in amplitude, about 55–65 dB. This indicates the acticities become even more sustained and energetic than that of 2-17h.

Taken together, the increase in long-duration and high-amplitude events in the later hours is consistent with the literature on corrosion AE where metastable pitting or film rupture gives way to more sustained interfacial activity. For eample, pit growth, film delamination, and gas evolution. Prior studies on stainless steels report that AE energy and large-amplitude events rise as pitting stabilizes and propagates. Prior studies on stainless steels report that AE energy and large-amplitude events rise as pitting stabilizes and propagates [49]. Meanwhile, hydrogen bubble nucleation—growth—detachment at active sites can generate AE in the 120–350 kHz band—overlapping the present sensor's resonance—so an increased density of bubbles and detachment events later in the experiment would manifest primarily as longer,

stronger AE without a systematic PF shift, exactly as observed in these figures [73], [77].

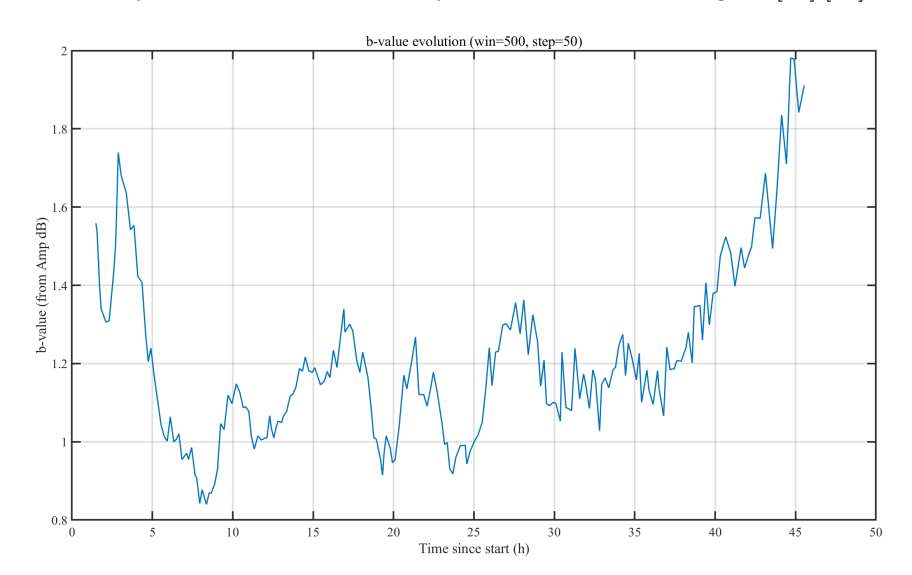


Figure 23: b-value evolution

Figure 23 illustrates the temporal evolution of the acoustic emission-derived b-value, calculated based on amplitude distributions using a moving window approach (window = 500, step = 50). The entire curve can be subdivided into three distinct stages.

In the early immersion stage (0–7 h), the b-value fluctuates around 1.4–1.6 before dropping sharply to values near 0.9. This reduction suggests that during the initiation of localized corrosion, particularly pit nucleation and the first instances of pit cover rupture, relatively energetic AE events dominate the signal population. Such behavior is consistent with the breakdown of the passive film and the onset of aggressive localized attack in acidic chloride environments.

Between approximately 10 h and 39 h, the b-value stabilizes in the range of 1.0–1.3 with intermittent fluctuations. This regime likely corresponds to the metastable growth and repassivation of pits, during which a mixture of low- and medium-energy AE events is generated. These events may arise from hydrogen bubble nucleation and detachment, fine-scale rupture of passive films, and small debris release, producing a balance between frequent low-energy emissions and occasional more energetic bursts.

In the later stage of the test (39–45 h), a pronounced upward trend is observed, with the b-value rising above 1.8 by the end of the exposure. This increase indicates a growing predominance of low-energy AE signals, which may correspond to stabilized corrosion processes dominated by frequent but relatively mild events such as continuous hydrogen bubbling. The concurrent decrease in the relative frequency of high-amplitude bursts suggests that catastrophic rupture events become less common, possibly due to the transition from active pit propagation to a more generalized corrosion regime or the accumulation of corrosion products that dampen sudden pit-cover failures.

Overall, the observed b-value evolution reflects a three-stage corrosion process: (i) an initiation stage dominated by high-energy AE signals linked to passive film breakdown and pit nucleation, (ii) an intermediate metastable regime with mixed AE activity, and (iii) a late stage characterized by a predominance of low-energy events associated with stabilized hydrogen evolution and sustained pit activity. This interpretation is consistent with the AE peak frequency distribution results, where the around 160 kHz resonance-dominated band was found across amplitude groups, indicating that the dominant mechanism (which is likely hydrogen bubble dynamics) persisted while the amplitude balance shifted as corrosion evolved.

6.4 EN results

6.4.1 EN raw data

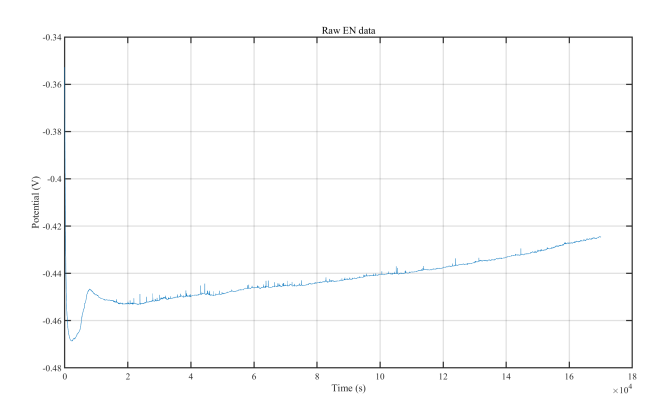


Figure 24: Raw EN data

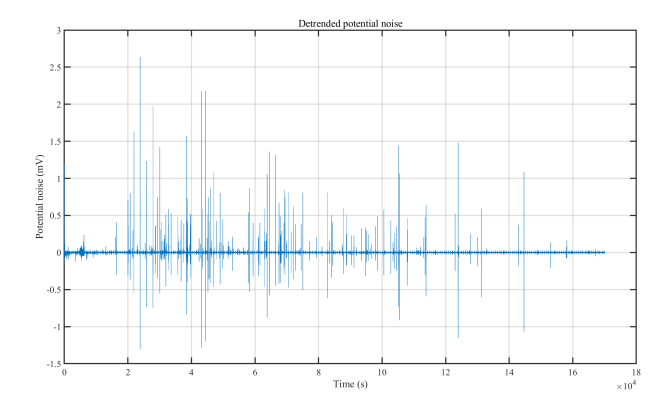


Figure 25: Detrended potential noise

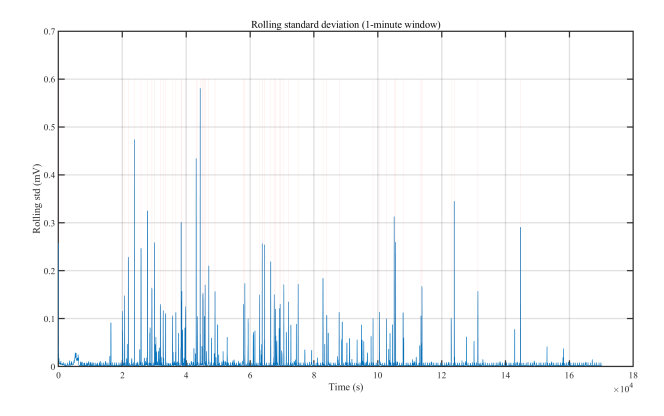


Figure 26: Rolling standard deviation

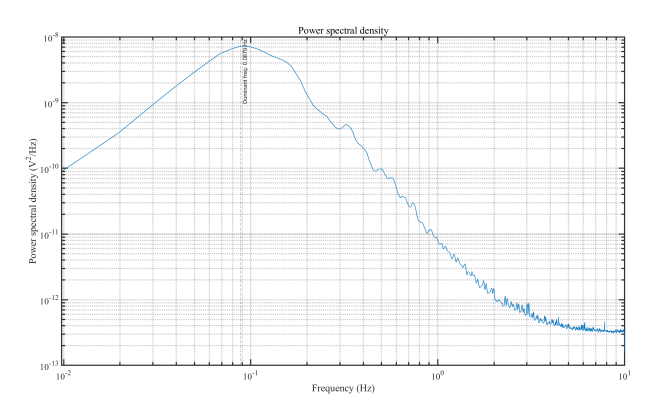


Figure 27: Power spectral density

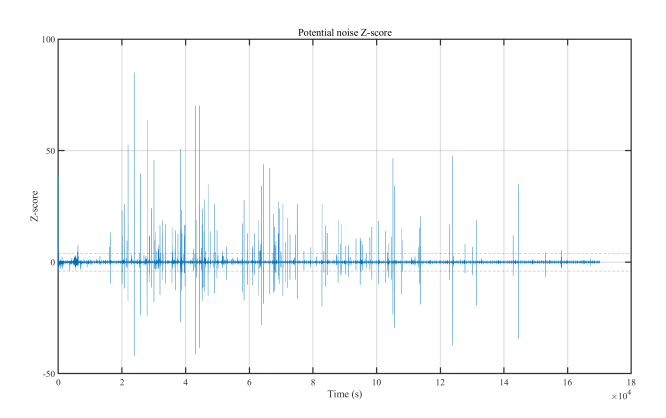


Figure 28: Potential noise Z-score

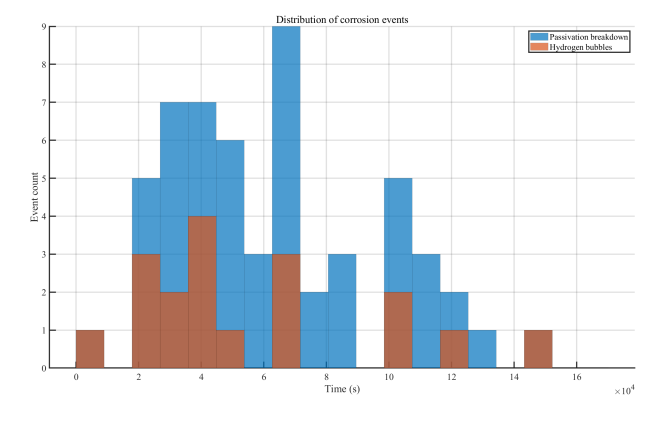


Figure 29: Distribution of possible passive film events and hydrogen bubble events

Figure 24 to Figure 29 present the analysis on EN data. The raw potential is decomposed into a slowly varying baseline (about 10 s moving average) and a fast noise residual by subtraction. This soft high-pass step suppresses drift/very-low-frequency processes so that subsequent statistics and PSD are not dominated by baseline wander [78], [68]. At open circuit, metastable pit activation on AISI 304 usually produces downward potential transients, because a sudden increase in local anodic dissolution drives the mixed potential to less noble values. In Figure 25, however, many upward spikes are also observed. These could be to cathodic inhibition by hydrogen bubbles in the acidic chloride electrolyte. Within the mixed-potential framework, the OCP satisfies $i_a(E) = i_c(E)$. A rapid decrease in the available cathodic area (bubble nucleation/coverage) lowers i_c at fixed E; to re-establish $i_a = i_c$, the potential shifts positively by $\Delta E > 0$ (noble direction), giving upward spikes. Conversely, brief depassivation/film-rupture events increase i_a and generate the expected downward excursions. The coexistence of both polarities therefore reflects alternating dominance of anodic (pit/film-rupture) and cathodic (bubble blocking/unblocking) processes—consistent with the later-stage, H₂-dominated regime indicated elsewhere in this study.

In Figure 27, the observed decline of the PSD toward the lowest frequencies is interpreted as a methodological consequence of detrending and finite-length Welch estimation (effective high-pass behavior), rather than the absence of slow corrosion dynamics[79]. The overall shape accords with literature on chloride-induced pitting EN: a broad maximum near 10^{-1} Hz linked to film rupture or repassivation kinetics, a $1/f^{\beta}$ range associated with bursty metastable-pit transients (with roll-off slope tied to transient differentiability), and a high-frequency flattening at the measurement noise floor[80],[68]. This agreement supports the interpretation used here.

Based on these conditions, a MATLAB script was developed to distinguish between the time periods potentially corresponding to passive film rupture and hydrogen bubble activity. The results are shown in Table 2 and table 3, which present the recognized passive film breakdown events and hydrogen bubble events.

Table 2: Possible passive film breakdown in the EN data

Start Time (s)	End Time (s)	Peak Time (s)
20 006.3	20 065.5	20 048.4
20680.3	20740.5	20716.3
21878.6	21940.3	21933.4
23809.7	23875.2	23847.8
25838.8	25901.8	25864.2
27881.0	27945.2	27926.9
29239.9	29300.8	29258.9
30033.5	30097.0	30088.4
31921.5	31980.7	31975.9
32773.1	32831.5	32826.1
33557.4	33614.3	33594.6
35725.7	35778.9	35744.7
36728.2	36785.1	36780.3
38388.9	38453.5	38447.1
38620.3	38681.1	38671.7
39813.0	39869.5	39815.8
43092.6	43157.8	43138.8
43475.6	43513.8	43499.2
44368.0	44445.2	44395.7
45169.0	45229.7	45223.0
45254.5	45314.9	45265.4
45722.3	45778.0	45739.8
45904.7	45965.5	45946.0
47041.1	47102.7	47095.4
48999.2	49059.7	49052.1
57881.4	57940.9	57903.5
58331.2	58392.2	58383.2
59376.9	59387.7	59384.0
62978.0	63039.5	62998.8
63787.3	63851.4	63834.9
64498.2	64561.0	64537.4
66430.6	66491.8	66482.5
67537.5	67597.9	67573.8
67905.6	67963.9	67937.7
69247.4	69306.9	69298.4
69417.3	69477.0	69441.1
70554.7	70615.9	70576.9
72032.8	72092.6	72071.3
75036.0	75097.0	75073.6
82817.8	82879.9	82846.1
83995.2	84051.7	84006.0
87 871.5	87929.7	87920.4
	-	

 $Continued\ on\ next\ page$

Table 2 (continued)

Start Time (s)	End Time (s)	Peak Time (s)
98 481.5	98534.5	98515.4
100526.0	100584.0	100557.0
102703.0	102757.0	102745.0
105101.0	105166.0	105148.0
105525.0	105589.0	105563.0
107898.0	107955.0	107936.0
113507.0	113564.0	113522.0
113809.0	113871.0	113814.0
122957.0	123012.0	122967.0
123901.0	123966.0	123957.0
131313.0	131374.0	131362.0
144 632.0	144 697.0	144 688.0

Table 3: Possible hydrogen-bubble events in EN data

Start Time (s)	End Time (s)	Peak Time (s)
21 909.3	21 910.3	21 909.6
23842.4	23844.6	23842.9
25870.1	25871.0	25870.4
27913.4	27915.0	27913.8
30065.6	30066.9	30066.3
38421.1	38422.6	38421.6
43125.2	43127.5	43125.8
44400.5	44402.5	44400.9
44412.5	44414.7	44413.1
47071.6	47072.5	47071.8
63820.3	63820.8	63820.5
64529.3	64530.7	64529.8
66460.6	66461.6	66460.9
105134.0	105136.0	105135.0
105557.0	105558.0	105558.0
123933.0	123936.0	123934.0
144 665.0	144 666.0	144 666.0

6.5 Correlating EN and AE results with the corrosion process

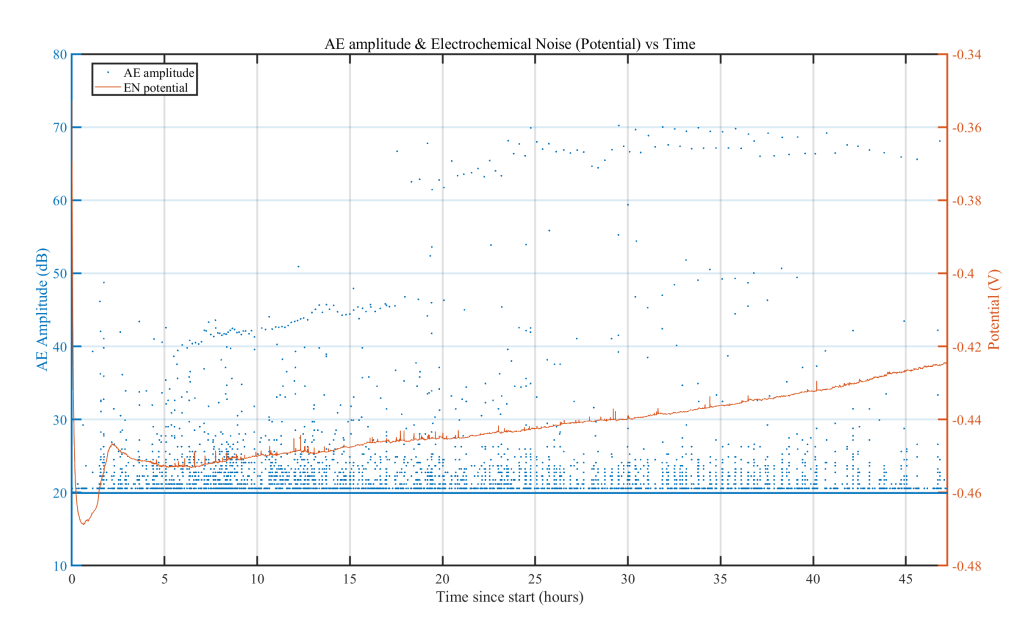


Figure 30: AE and EN combined result

Figure 30 presents the AE and EN results together. After an initial immersion transient during the first 2 hours, the EN potential drifts steadily to more positive values with occasional spikes. In parallel, there is a clear rise in the maximum amplitude from AE side. Early in the test most hits lie below 40–45 dB, whereas from 25 hours onward numerous events reach 60–70 dB. Several AE bursts temporally coincide with sharp potential excursions. This may indicate intermittent surface instabilities, while the overall trend shows that localized, energetic activity intensifies even as the bulk potential evolves smoothly.

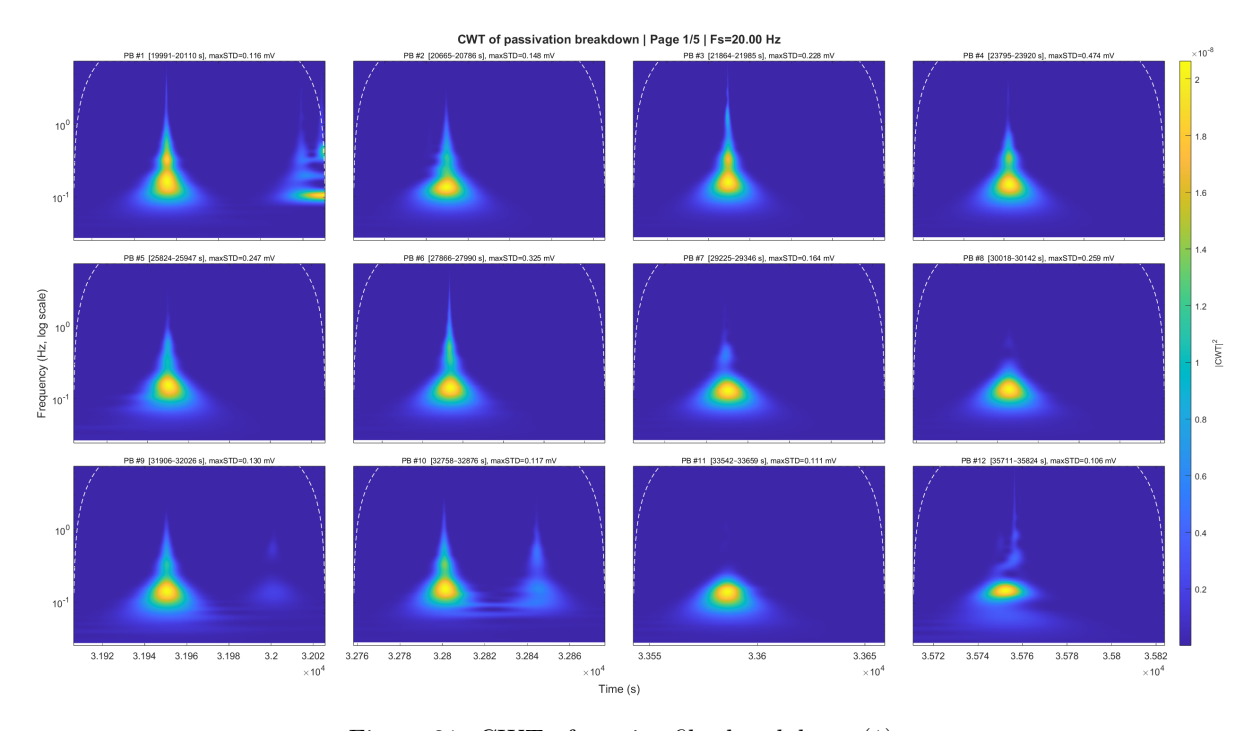


Figure 31: CWT of passive film breakdown (1)

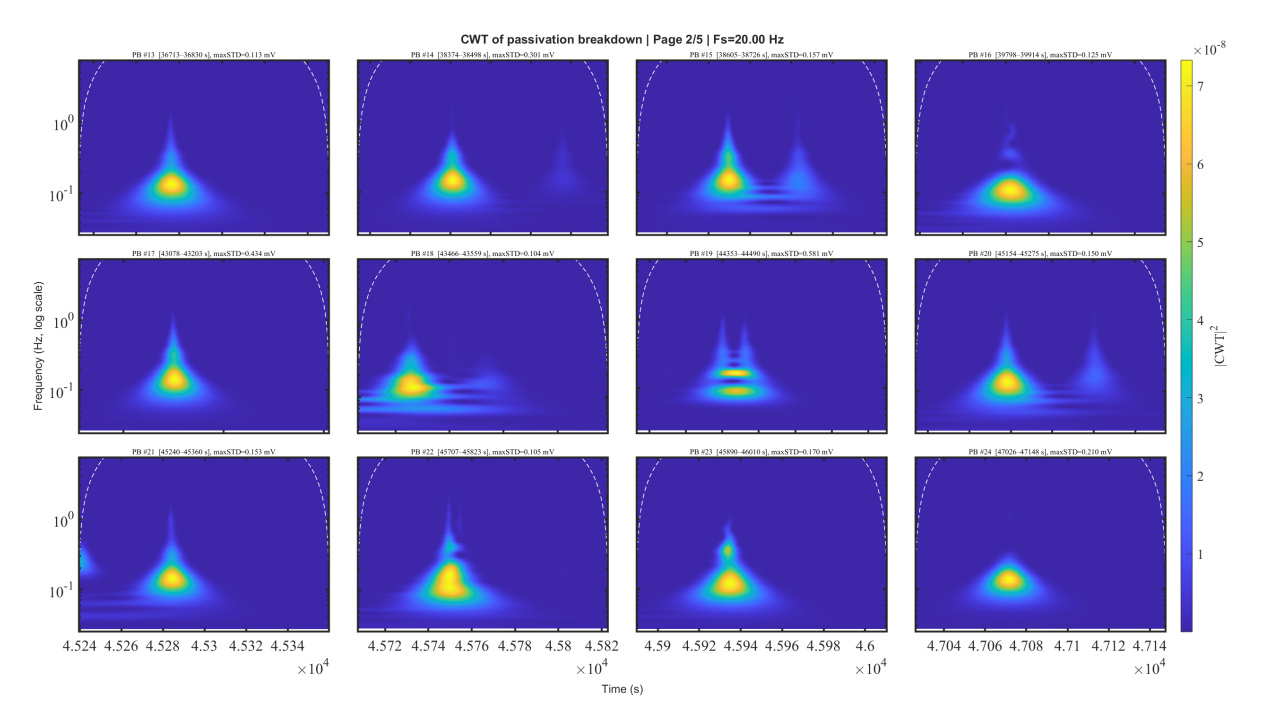


Figure 32: CWT of passive film breakdown (2)

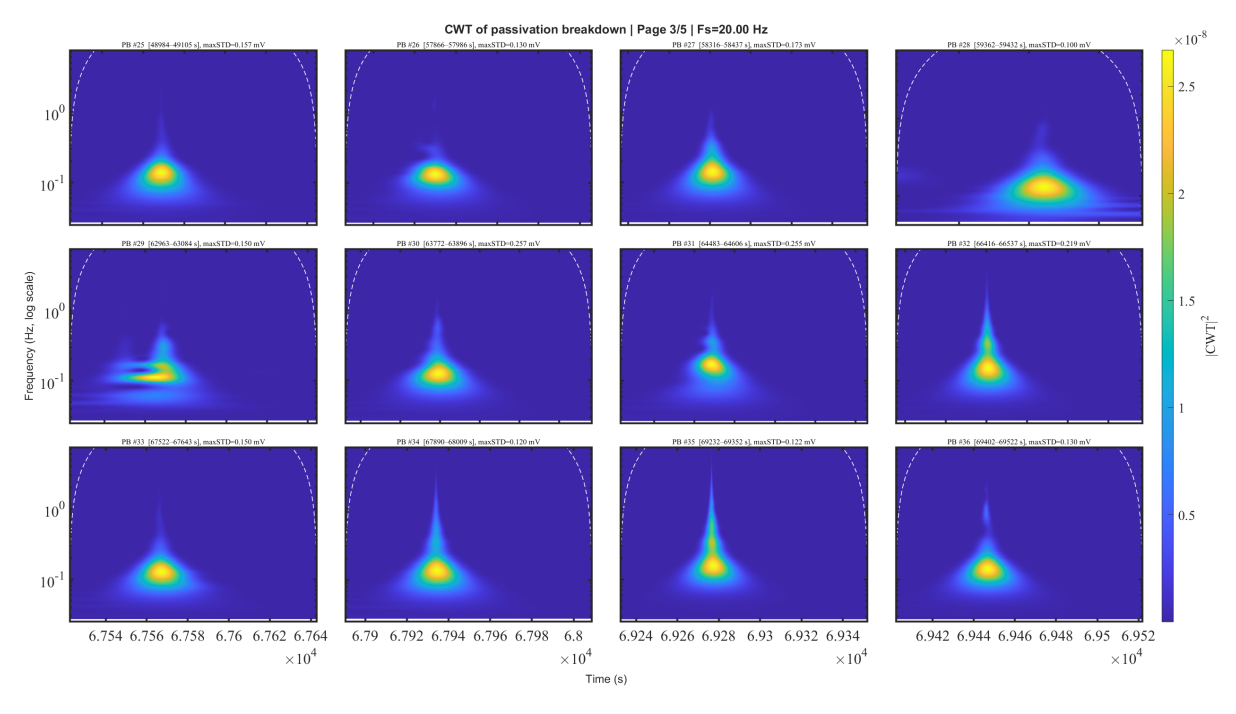


Figure 33: CWT of passive film breakdown (3)

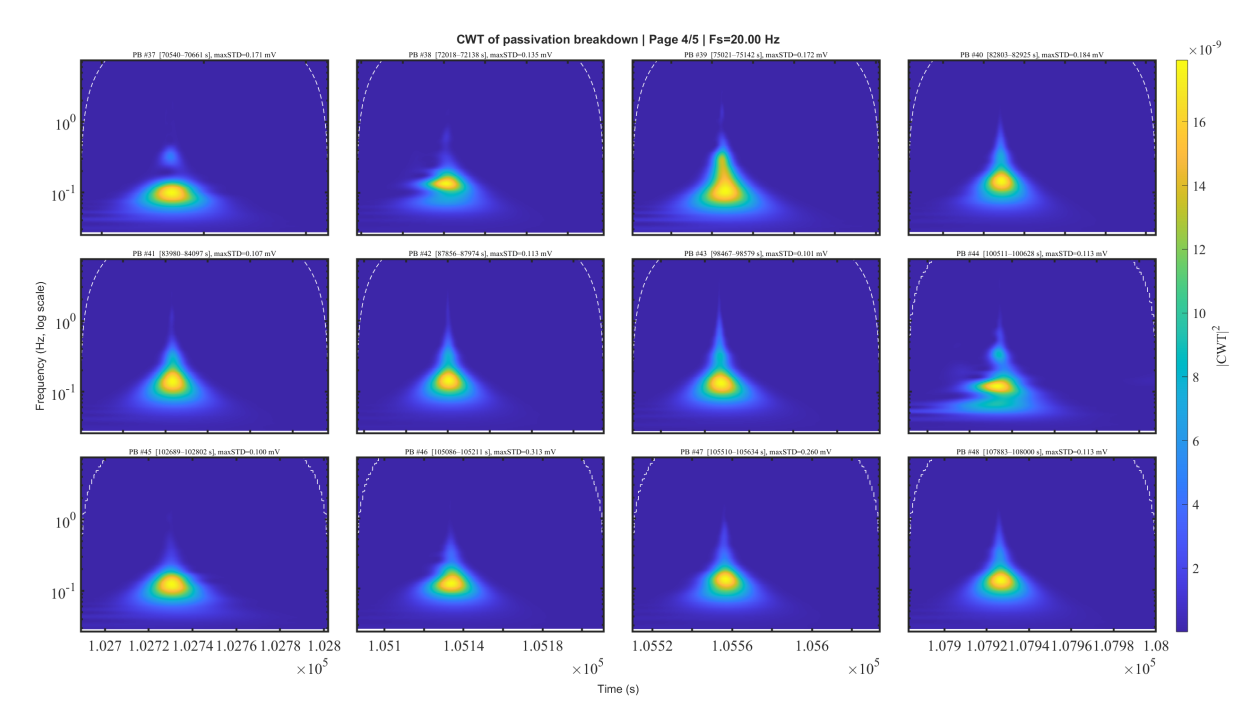


Figure 34: CWT of passive film breakdown (4)

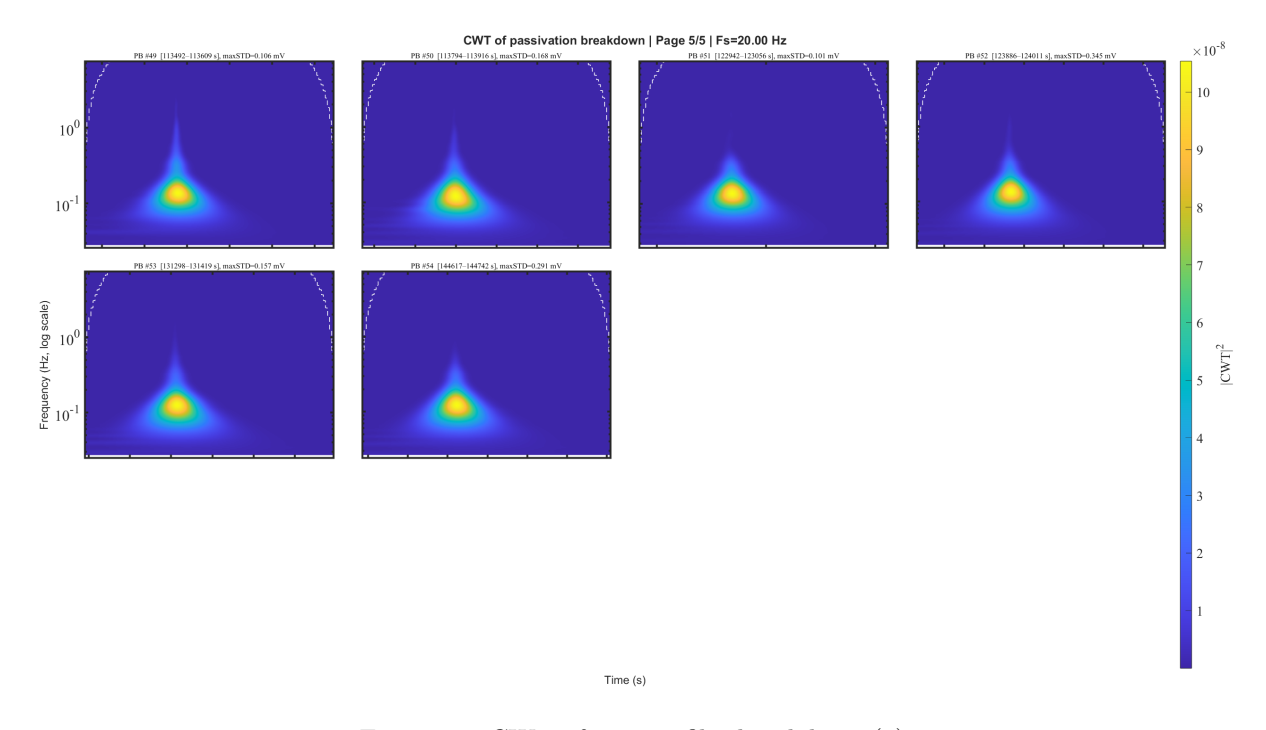


Figure 35: CWT of passive film breakdown (5)

Figure 35 present the CWT results of the passive film breakdown events in Table 2. Each passive film breakdown window shows a highly consistent 'volcano' time-frequency signature. Energy is strongly concentrated at low frequencies ($\sim 0.08-0.3$ Hz) with a narrow vertical ridge that tapers upward in frequency. The events last for a few seconds and in many cases display faint secondary bands up to ~ 1 Hz or short multi-pulse structures. This matches a rapid passive film breakdown followed by slower repassivation in the time domain. Stronger events exhibit a fuller and brighter low-frequency kernel and are more likely to carry high-frequency streaks or successive pulses. Importantly, the dominant frequency band does not drift systematically across pages, implying that the intrinsic passivation breakdown time scale remains fairly stable over the test. Overall, the CWT results confirms that passive film breakdown is dominated by low frequencies. This agrees with previous studies [81], [68], [82].

Figure 36 to Figure 40 present AE signals of passive film breakdown events in Table 2. Across all five groups the AE hits detected inside the time windows show a very consistent pattern. Most points cluster at peak frequency around 165–172 kHz with short durations from 200 to 600 μ s. The amplitudes vary from 20 to 40 dB. As discussed previously, this narrow PF band could be influenced by the sensor. Consequently, duration, amplitude and hit count are the useful indicators of activity level.

Window-to-window variability appears mainly in event abundance n, upper-tail duration, and amplitude. Several windows are sparse ($n \approx 3$ –8) with only short, low-amplitude hits, while others (e.g., #6, #8, #16, #19, #31, #33, #36–37, #53–54) contain more hits, higher amplitudes (approaching 40–45 dB), and occasional long-duration outliers (≥ 1 –3 ms). A few windows also show lower-PF points (≈ 50 –120 kHz) that tend to coincide with longer durations. These may due to the overlapping of signals. Taken together, the AE results looks like bursts of short and resonant hits punctuated by sporadic longer or stronger events. This may be consistent with local film rupture and repassivation and sometimes leading to clustered micro-failures. Besides, later windows exhibit more and stronger hits and a higher upper peak value of duration. This also agrees with the previous EN results.

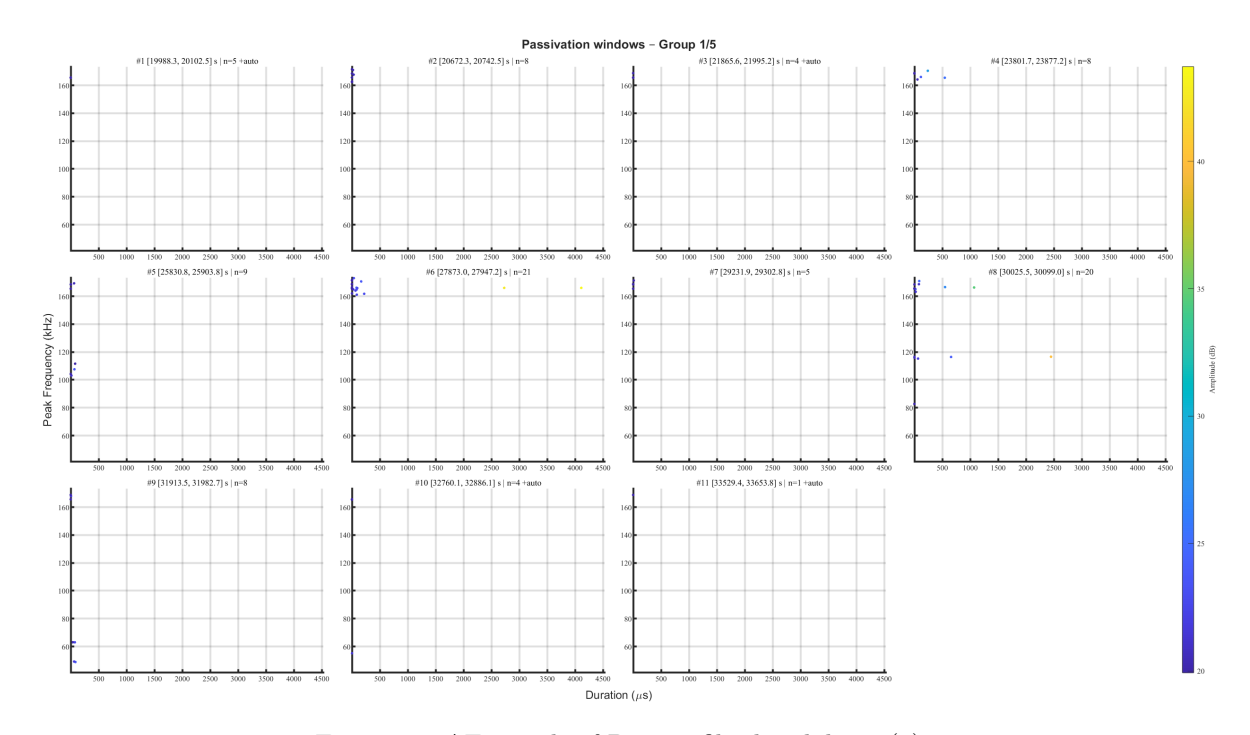


Figure 36: AE signals of Passive film breakdown (1)

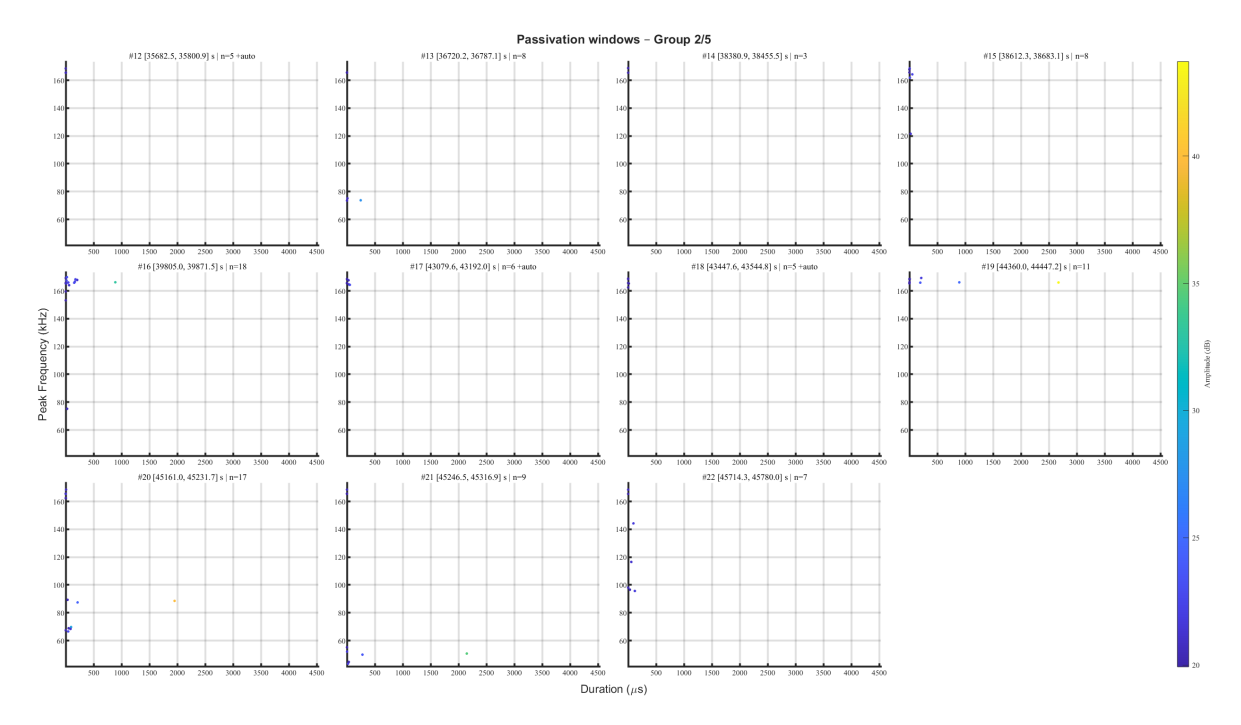


Figure 37: AE signals of Passive film breakdown (2)

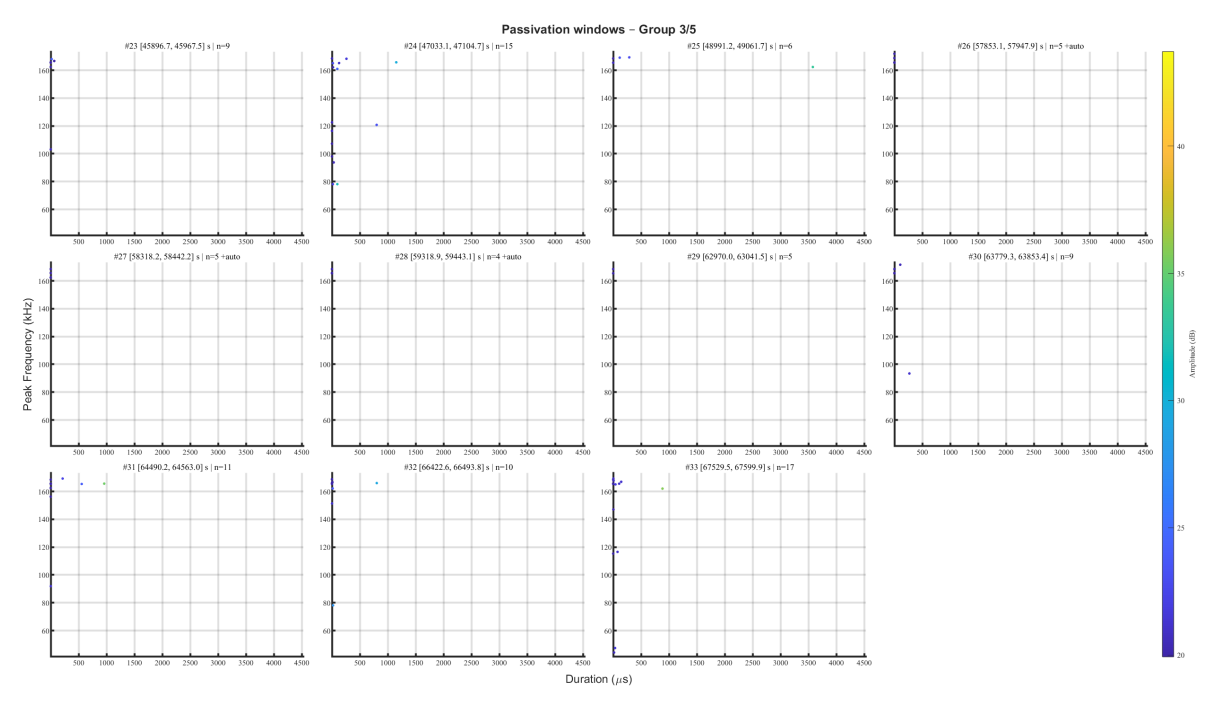


Figure 38: AE signals of Passive film breakdown (3)

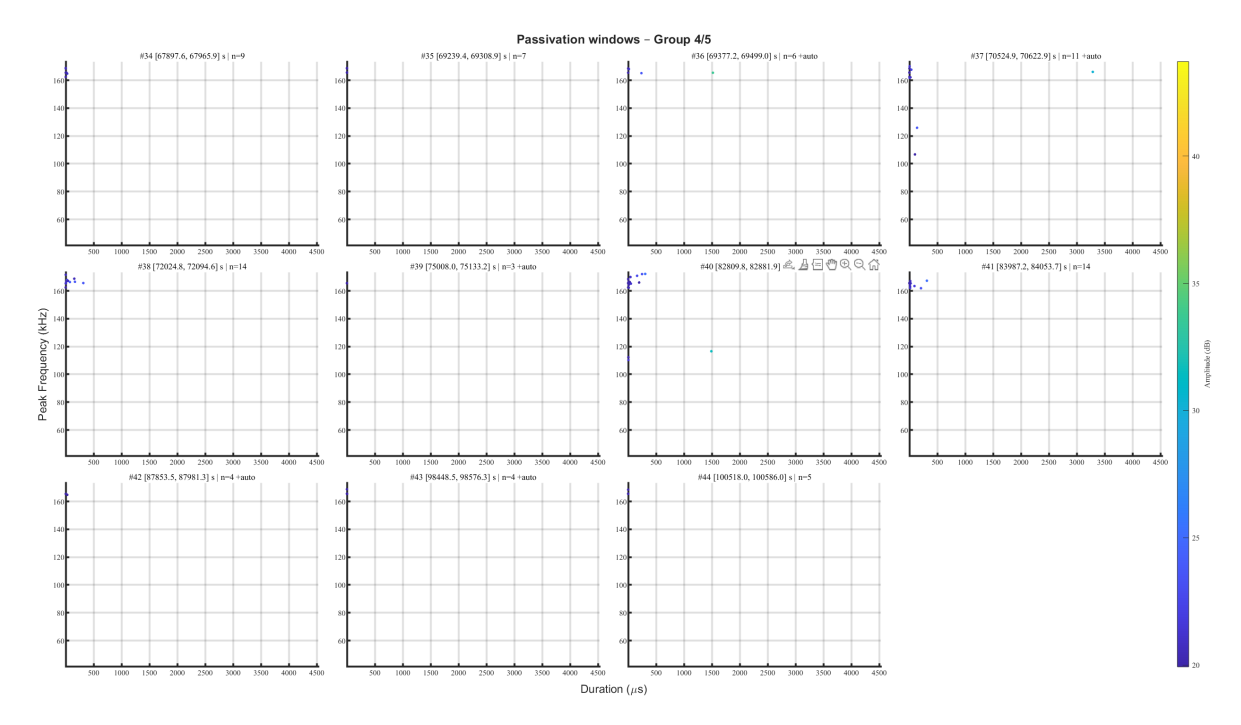


Figure 39: AE signals of Passive film breakdown (4)

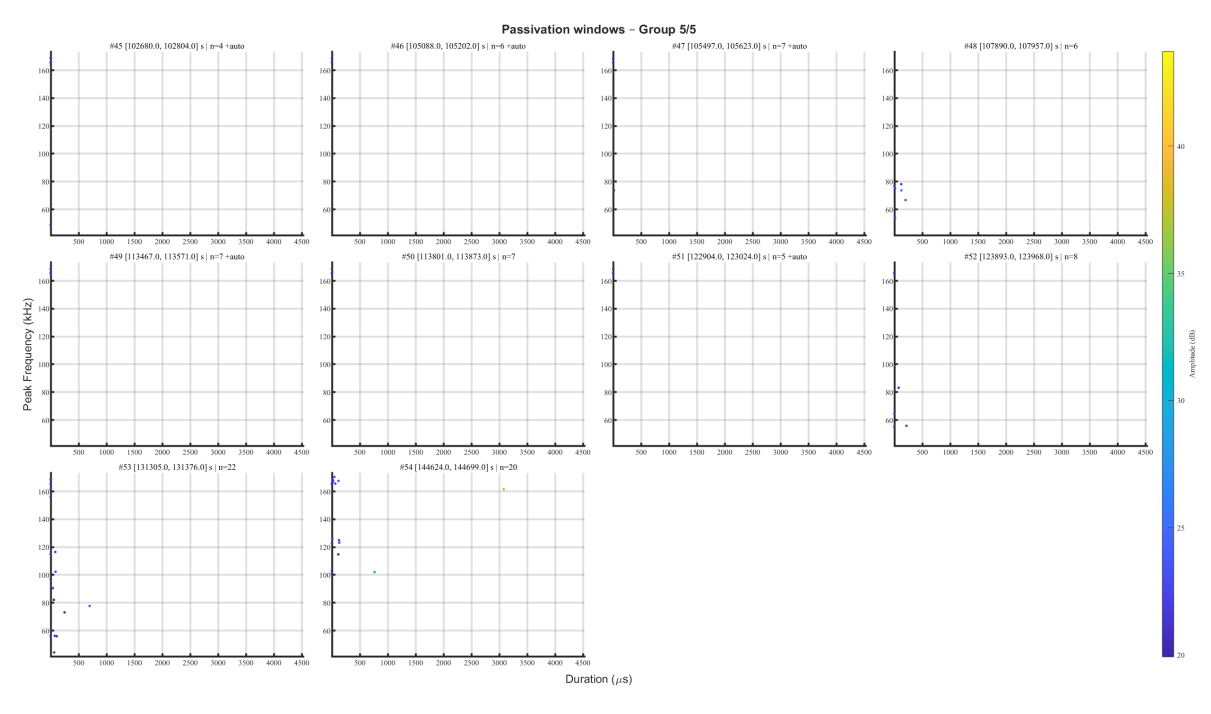


Figure 40: AE signals of Passive film breakdown (5)

Figure 41 and Figure 42 present AE signals of hydrogen bubble events shown in Table 3. In contrast with AE signals of passive film breakdown, in the hydrogen-bubble windows, although the AE hits are still dominated by the sensor resonance at 165–172 kHz, but they show greater scatter toward lower PF than the passivation windows. Several windows contain points at 60–140 kHz. Meanwhile, longer duration outliers (up to 3–4.5 ms) occur more frequently. It could be also observed that hits tend to appear in clusters. This could be related to bubble nucleation, growth, and detachment[73],[83].

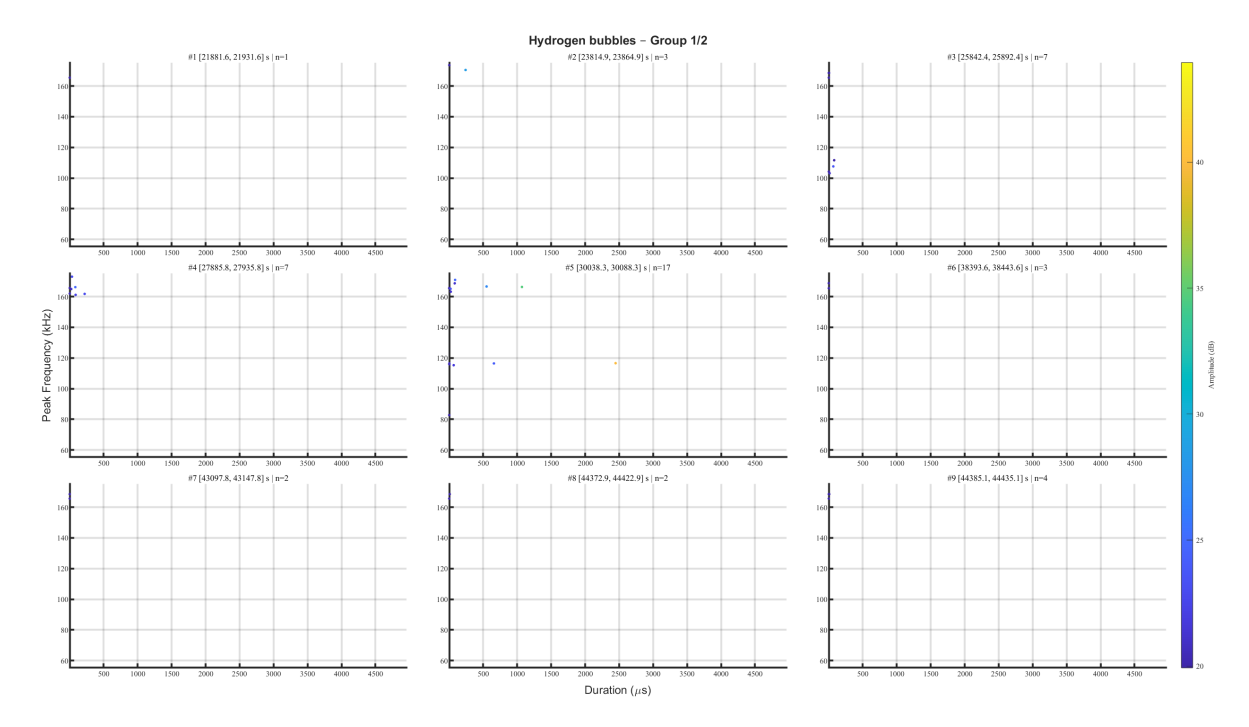


Figure 41: AE signals of hydrogen bubble events page 1

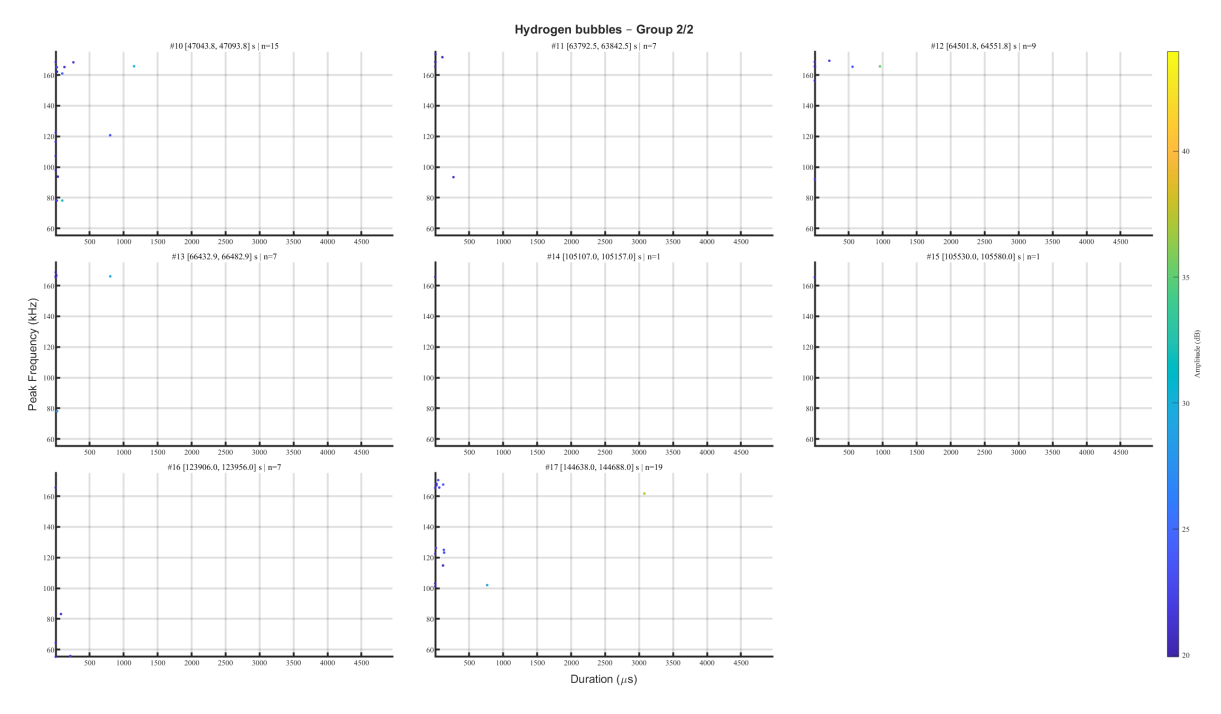


Figure 42: AE signals of hydrogen bubble events page $2\,$

7 Conclusions

- 1. This study established acoustic emission (AE) and electrochemical noise (EN) in-situ co-monitoring method for monitoring pitting of AISI 304 stainless steel in 3.5 wt% NaCl (pH = 2). The setup synchronizes acoustic hits with electrochemical transients and is suitable for long-duration observation.
- 2. Microscopy shows corrosion is dominated by highly localized pitting and also with general attack. In later stages, abundant surface bubbles are observed, offering a plausible AE source via hydrogen nucleation—growth—detachment.
- 3. AE evolves in stages: 1 h of near-silence, followed by intermittent events mainly at 40–50 dB. After 16 h, events with higher amplitude and longer duration become frequent. Beyond 30 h, maximum durations reach 17 ms. The b-value exhibits a three-stage trend: early prominence of higher-energy events, a mixed regime mid-test, and a late regime dominated by lower-energy but higher-rate events, consistent with sustained H₂ evolution and stable pit activity.
- 4. After detrending, EN analysis with statistical criteria resolves passive-film rupture windows and hydrogen bubble event windows. Continuous wavelet transforms show that film-rupture episodes concentrate low-frequency energy with a volcano-like pattern.
- 5. Cross-modal analysis of the AE and EN records reveals that episodes linked to passive-film rupture are dominated by short, low-amplitude bursts. And hydrogen-dominated episodes exhibit longer, clustered events.
- 6. R15 α sensor (peak sensitivity \sim 150 kHz) projects different source mechanisms into the 165–172 kHz region. Hence, peak frequency alone is insufficient for source discrimination.

8 Recommendations for future research

The present study has demonstrated the potential of combining acoustic emission and electrochemical noise techniques for in-situ monitoring of pitting corrosion in stainless steel and for elucidating possible AE source mechanisms. Nevertheless, there are still several questions and technical challenges remain. The following is some recommendations for the future research.

Although time-synchronized AE–EN analysis improves source discrimination, the physical origins of many AE events remain ambiguous. Future studies could integrate AE and EN with complementary high-resolution visualization techniques, such as in-situ optical microscopy, to directly link individual AE bursts to observable corrosion phenomena (such as those reactions about hydrogen bubble or pit cover detachment).

Meanwhile, the complexity and overlap of corrosion-related AE waveforms need more accurate data processing. Future work could use deep learning models trained on labeled datasets of known corrosion events to enhance automated AE signal classification. Combining time–frequency analysis with clustering or supervised learning may help further improve the accuracy of source attribution in noisy environments.

While this study focused on AISI 304 stainless steel in acidic chloride solutions, it is also interesting to explore whether the observed AE–EN correlations and signal patterns hold for other alloys (such as duplex stainless steels, aluminum alloys) and under different service-relevant environments, such as neutral pH seawater, high-temperature conditions, or under mechanical stress.

References

- [1] Gerhardus Koch, Jeff Varney, Neil Thompson, Oliver Moghissi, Melissa Gould, and Joe Payer. International measures of prevention, application, and economics of corrosion technologies study. *NACE int*, 216(3), 2016.
- [2] Pierre R Roberge. Corrosion inspection and monitoring. John Wiley & Sons, 2007.
- [3] Luigi Calabrese and Edoardo Proverbio. A review on the applications of acoustic emission technique in the study of stress corrosion cracking. *Corrosion and Materials Degradation*, 2(1):1–30, 2020.
- [4] Kateryna Popova and Tomáš Prošek. Corrosion monitoring in atmospheric conditions: a review. *Metals*, 12(2):171, 2022.
- [5] Chloé Comas, François Huet, Kieu Ngo, Marion Fregonese, Hassane Idrissi, and Bernard Normand. Corrosion propagation monitoring using electrochemical noise measurements on carbon steel in hydrogenocarbonated solution containing chloride ions. *Corrosion Science*, 193:109885, 2021.
- [6] Haofeng Zhang, Zhiqin Wu, Yang Chen, Kaixuan Feng, Hong Yan, Honggun Song, Chao Luo, and Zhi Hu. Real-time monitoring of the corrosion behaviour of the 304ss in hcl solution using bpnn with joint image recognition and electrochemical noise. *Corrosion Science*, 228:111779, 2024.
- [7] Zhina Razaghi, Milad Rezaei, and Seyed Hadi Tabaian. Electrochemical noise and impedance study on the corrosion of electroplated ni-cr coatings in hbf4 aqueous solution. *Journal of Electroanalytical Chemistry*, 859:113838, 2020.
- [8] Jian Xu, Xinqiang Wu, and En-Hou Han. Acoustic emission during pitting corrosion of 304 stainless steel. *Corrosion Science*, 53(4):1537–1546, 2011.
- [9] Marion Fregonese, Hassane Idrissi, Henri Mazille, Luc Renaud, and Y Cetre. Initiation and propagation steps in pitting corrosion of austenitic stainless steels: monitoring by acoustic emission. *Corrosion science*, 43(4):627–641, 2001.
- [10] F Mansfeld and PJ Stocker. Acoustic emission from corroding electrodes. *Corrosion*, 35(12):541–544, 1979.
- [11] Stefan Krakowiak and Kazimierz Darowicki. Electrochemical and acoustic emission studies of aluminum pitting corrosion. *Journal of Solid State Electrochemistry*, 13:1653–1657, 2009.
- [12] Marion Fregonese, Hassane Idrissi, Henri Mazille, L Renaud, and Y Cetre. Monitoring pitting corrosion of aisi 316l austenitic stainless steel by acoustic emission technique: choice of representative acoustic parameters. *Journal of materials science*, 36:557–563, 2001.
- [13] R Winston Revie. Corrosion and corrosion control: an introduction to corrosion science and engineering. John Wiley & Sons, 2008.
- [14] Taiwo W Quadri, Ekemini D Akpan, Lukman O Olasunkanmi, Omolola E Fayemi, and Eno E Ebenso. Fundamentals of corrosion chemistry. In *Environmentally sustainable corrosion inhibitors*, pages 25–45. Elsevier, 2022.
- [15] Abdenacer Berradja. Electrochemical techniques for corrosion and tribocorrosion monitoring: methods for the assessment of corrosion rates. In *Corrosion inhibitors*. IntechOpen, 2019.
- [16] SA Abd El-Maksoud. The effect of organic compounds on the electrochemical behaviour of steel in acidic media. a review. *International Journal of Electrochemical Science*, 3(5):528–555, 2008.
- [17] Bogumił Eugeniusz Brycki, Iwona H Kowalczyk, Adrianna Szulc, Olga Kaczerewska, and Marta Pakiet. Organic corrosion inhibitors. Corrosion inhibitors, principles and recent applications, 3:33, 2018.
- [18] Edward Ghali, Wolfgang Dietzel, and Karl-Ulrich Kainer. General and localized corrosion of magnesium alloys: a critical review. *Journal of materials engineering and performance*, 13:7–23, 2004.
- [19] Abdel Salam Hamdy Makhlouf. Intelligent stannate-based coatings of self-healing functionality for magnesium alloys. In *Intelligent coatings for corrosion control*, pages 537–555. Elsevier, 2015.

- [20] S Harsimran, K Santosh, and K Rakesh. Overview of corrosion and its control: A critical review. *Proc. Eng. Sci*, 3(1):13–24, 2021.
- [21] S. Hiromoto. 4 corrosion of metallic biomaterials. In Mitsuo Niinomi, editor, *Metals for Biomedical Devices*, Woodhead Publishing Series in Biomaterials, pages 99–121. Woodhead Publishing, 2010.
- [22] GS Frankel. Pitting corrosion of metals: a review of the critical factors. *Journal of the Electrochemical society*, 145(6):2186, 1998.
- [23] Fuad Khoshnaw and Rolf Gubner. Part i: General aspects of corrosion, corrosion control, and corrosion prevention. In *Corrosion Atlas Case Studies*, Corrosion Atlas Series, pages xxv–xli. Elsevier, 2020.
- [24] GS Frankel and N Sridhar. Understanding localized corrosion. Materials today, 11(10):38-44, 2008.
- [25] Nihal U Obeyesekere. Pitting corrosion. Trends in oil and gas corrosion research and technologies, pages 215–248, 2017.
- [26] NJ Laycock, J Stewart, and RC Newman. The initiation of crevice corrosion in stainless steels. Corrosion science, 39(10-11):1791–1809, 1997.
- [27] Sachiko Hiromoto. 4 corrosion of metallic biomaterials. In Mitsuo Niinomi, editor, *Metals for Biomedical Devices (Second Edition)*, Woodhead Publishing Series in Biomaterials, pages 131–152. Woodhead Publishing, second edition edition, 2019.
- [28] Nadim James Hallab, Carlo Messina, Anastasia Skipor, and Joshua J Jacobs. Differences in the fretting corrosion of metal–metal and ceramic–metal modular junctions of total hip replacements. *Journal of Orthopaedic Research*, 22(2):250–259, 2004.
- [29] Danieli C Rodrigues, Robert M Urban, Joshua J Jacobs, and Jeremy L Gilbert. In vivo severe corrosion and hydrogen embrittlement of retrieved modular body titanium alloy hip-implants. Journal of Biomedical Materials Research Part B: Applied Biomaterials: An Official Journal of The Society for Biomaterials, The Japanese Society for Biomaterials, and The Australian Society for Biomaterials and the Korean Society for Biomaterials, 88(1):206–219, 2009.
- [30] Zozia Szklarska-Smialowska et al. Pitting corrosion of metals. (No Title), 1986.
- [31] RC Newman, HS Isaacs, and B Alman. Effects of sulfur compounds on the pitting behavior of type 304 stainless steel in near-neutral chloride solutions. *Corrosion*, 38(5):261–265, 1982.
- [32] Surinder Pal, Shailendra Singh Bhadauria, and Pramod Kumar. Pitting corrosion behavior of f304 stainless steel under the exposure of ferric chloride solution. *Journal of Bio-and Tribo-Corrosion*, 5:1–13, 2019.
- [33] Jakub Tkacz, Jozef Minda, Stanislava Fintová, and Jaromír Wasserbauer. Comparison of electrochemical methods for the evaluation of cast az91 magnesium alloy. *Materials*, 9(11):925, 2016.
- [34] Elif Burcu Bahadır and Mustafa Kemal Sezgintürk. A review on impedimetric biosensors. *Artificial cells, nanomedicine, and biotechnology,* 44(1):248–262, 2016.
- [35] Hend S Magar, Rabeay YA Hassan, and Ashok Mulchandani. Electrochemical impedance spectroscopy (eis): Principles, construction, and biosensing applications. *Sensors*, 21(19):6578, 2021.
- [36] J Benavente. Electrochemical impedance spectroscopy as a tool for electrical and structural characterizations of membranes in contact with electrolyte solutions. In *Recent Advances in Multidisci-plinary Applied Physics*, pages 463–471. Elsevier, 2005.
- [37] VF Lvovich. Electrochemical impedance spectroscopy (eis) applications to sensors and diagnostics. Encyclopedia of applied electrochemistry, pages 485–507, 2014.
- [38] Jesús Manuel Jáquez-Muñoz, Citlalli Gaona-Tiburcio, Jose Cabral-Miramontes, Demetrio Nieves-Mendoza, Erick Maldonado-Bandala, Javier Olguín-Coca, Francisco Estupinán-López, Luis Daimir López-León, José Chacón-Nava, and Facundo Almeraya-Calderón. Frequency analysis of transients in electrochemical noise of superalloys waspaloy and ultimet. Metals, 11(5):702, 2021.

- [39] RA Cottis. Simulation of electrochemical noise due to metastable pitting. J. Corr. Sci. Eng, 3, 2000.
- [40] Christopher B Scruby. An introduction to acoustic emission. *Journal of Physics E: Scientific Instruments*, 20(8):946, 1987.
- [41] Yunlong Wu, Jing Nong, Sui Yuan, Qi Guo, and Jian Xu. Acoustic emission behaviour during the evolution of a single pit on stainless steels. *Corrosion Science*, 183:109308, 2021.
- [42] Bill Drafts. Acoustic wave technology sensors. *IEEE Transactions on microwave theory and techniques*, 49(4):795–802, 2001.
- [43] Álvaro Carrasco, Franco Méndez, Félix Leaman, and Cristián Molina Vicuña. Short review of the use of acoustic emissions for detection and monitoring of cracks. *Acoustics Australia*, 49:273–280, 2021.
- [44] Luigi Calabrese and Edoardo Proverbio. A review on the applications of acoustic emission technique in the study of stress corrosion cracking. *Corrosion and Materials Degradation*, 2(1):1–30, 2021.
- [45] Christian U Grosse, Masayasu Ohtsu, Dimitrios G Aggelis, and Tomoki Shiotani. Acoustic emission testing: Basics for research-applications in engineering. Springer Nature, 2021.
- [46] Shigenori Yuyama, Y Hisamatsu, and T Kishi. Fundamental aspects of ae monitoring on corrosion fatigue processes in austenitic stainless steel. J. Mater. Energy Syst.; (United States), 5(4), 1984.
- [47] Asa Prateepasen, Chalermkiat Jirarungsatean, and Pongsak Tuengsook. Identification of ae source in corrosion process. *Key Engineering Materials*, 321:545–548, 2006.
- [48] RH Jones and MA Friesel. Acoustic emission during pitting and transgranular crack initiation in type 304 stainless steel. *Corrosion*, 48(09), 1992.
- [49] Kaige Wu, Woo-Sang Jung, and Jai-Won Byeon. In-situ monitoring of pitting corrosion on vertically positioned 304 stainless steel by analyzing acoustic-emission energy parameter. *Corrosion science*, 105:8–16, 2016.
- [50] Mitsuharu Shiwa, Hiroyuki Masuda, Hisashi Yamawaki, Kaita Ito, and Manabu Enoki. In-situ observation and acoustic emission analysis for scc of mgcl2 droplet in sus304 stainless steel. *Materials Transactions*, 55(2):285–289, 2014.
- [51] Volodymyr Kietov, Marcel Mandel, and Lutz Krüger. Combination of electrochemical noise and acoustic emission for analysis of the pitting corrosion behavior of an austenitic stainless cast steel. Advanced Engineering Materials, 21(5):1800682, 2019.
- [52] Juliusz Orlikowski, A Jazdzewska, Robert Mazur, and Kazimierz Darowicki. Determination of pitting corrosion stage of stainless steel by galvanodynamic impedance spectroscopy. *Electrochimica Acta*, 253:403–412, 2017.
- [53] Marcel Mandel, Volodymyr Kietov, and Lutz Krüger. The corrosion behavior of high-alloy crmnni steels—a research work on electrochemical degradation in salt-and acid-containing environments. Austenitic TRIP/TWIP Steels and Steel-Zirconia Composites: Design of Tough, Transformation-Strengthened Composites and Structures, pages 557–584, 2020.
- [54] Marcel Mandel, Lutz Krüger, and Sabine Decker. Electrochemical corrosion studies of spark plasma sintered zirconia particle-reinforced high-alloy steel at different temperatures. Corrosion Science, 90:323–330, 2015.
- [55] Axel Homborg, Arjan Mol, and Tiedo Tinga. Corrosion classification through deep learning of electrochemical noise time-frequency transient information. *Engineering Applications of Artificial Intelligence*, 133:108044, 2024.
- [56] K Hladky and JL Dawson. The measurement of localized corrosion using electrochemical noise. Corrosion Science, 21(4):317–322, 1981.
- [57] K Hladky and JL Dawson. The measurement of corrosion using electrochemical 1f noise. *Corrosion Science*, 22(3):231–237, 1982.

- [58] AM Homborg, Tiedo Tinga, X Zhang, EPM Van Westing, PJ Oonincx, JHW De Wit, and JMC Mol. Time–frequency methods for trend removal in electrochemical noise data. *Electrochimica Acta*, 70:199–209, 2012.
- [59] DO Harris and HL Dunegan. Acoustic emission—5: Applications of acoustic emission to industrial problems. *Non-Destructive Testing*, 7(3):137–144, 1974.
- [60] H Mazille, R Rothea, and C Tronel. An acoustic emission technique for monitoring pitting corrosion of austenitic stainless steels. Corrosion Science, 37(9):1365–1375, 1995.
- [61] Kaige Wu and Jai-Won Byeon. Morphological estimation of pitting corrosion on vertically positioned 304 stainless steel using acoustic-emission duration parameter. *Corrosion Science*, 148:331–337, 2019.
- [62] H Bi, Z Li, D Hu, I Toku-Gyamerah, and Y Cheng. Cluster analysis of acoustic emission signals in pitting corrosion of low carbon steel: Clusteranalyse des schallemissionssignals bei lochkorrosion von niedrig legiertem stahl. *Materialwissenschaft und Werkstofftechnik*, 46(7):736–746, 2015.
- [63] Jian Li, Gang Du, Chen Jiang, and Shijiu Jin. The classification of acoustic emission signals of 304 stainless steel during stress corrosion process based on k-means clustering. Anti-Corrosion Methods and Materials, 59(2):76–80, 2012.
- [64] Sarjoon Alkhateeb, Filippo Riccioli, Felipe Leon Morales, and Lotfollah Pahlavan. Non-contact acoustic emission monitoring of corrosion under marine growth. Sensors, 23(1):161, 2022.
- [65] Gang Du, Jian Li, WK Wang, C Jiang, and SZ Song. Detection and characterization of stress-corrosion cracking on 304 stainless steel by electrochemical noise and acoustic emission techniques. Corrosion Science, 53(9):2918–2926, 2011.
- [66] C Jirarungsatian and A Prateepasen. Pitting and uniform corrosion source recognition using acoustic emission parameters. Corrosion Science, 52(1):187–197, 2010.
- [67] J Smulko et al. Methods of trend removal in electrochemical noise data—overview. *Measurement*, 131:569–581, 2019.
- [68] RA Cottis. Interpretation of electrochemical noise data. Corrosion, 57(3):265–285, 2001.
- [69] RA Cottis, MAA Al-Awadhi, H Al-Mazeedi, and S Turgoose. Measures for the detection of localized corrosion with electrochemical noise. *Electrochimica Acta*, 46(24-25):3665–3674, 2001.
- [70] Jesús Manuel Jáquez-Muñoz, Citlalli Gaona-Tiburcio, Ce Tochtli Méndez-Ramírez, Cynthia Martínez-Ramos, Miguel Angel Baltazar-Zamora, Griselda Santiago-Hurtado, Francisco Estupinan-Lopez, Laura Landa-Ruiz, Demetrio Nieves-Mendoza, and Facundo Almeraya-Calderon. Electro-chemical noise analysis: An approach to the effectivity of each method in different materials. Materials, 17(16):4013, 2024.
- [71] Peter D Welch. The use of fast fourier transform for the estimation of power spectra: A method based on time averaging over short, modified periodograms. *IEEE Transactions on audio and electroacoustics*, 15(2):70–73, 1967.
- [72] Fredric J Harris. On the use of windows for harmonic analysis with the discrete fourier transform. *Proceedings of the IEEE*, 66(1):51–83, 2005.
- [73] Volodymyr Kietov, Marcel Mandel, Lutz Krüger, and Alexei Vinogradov. Acoustic emission from gas bubbl e nucleation and breaking away from a flat surface. J. Acoust. Emiss, 35:274–280, 2018.
- [74] Kaige Wu, Kaita Ito, Ippei Shinozaki, Pornthep Chivavibul, and Manabu Enoki. A comparative study of localized corrosion and stress corrosion cracking of 13cr martensitic stainless steel using acoustic emission and x-ray computed tomography. *Materials*, 12(16):2569, 2019.
- [75] V Soltangharaei1a, JW Hill, Li Ai, R Anay, B Gree2b, M Bayat, and P Ziehl. Acoustic emission technique to identify stress corrosion cracking damage. Structural Engineering and Mechanics, 75(6):723-736, 2020.
- [76] Dandan Liu, Bin Wang, Han Yang, and Stephen Grigg. A comparison of two types of acoustic emission sensors for the characterization of hydrogen-induced cracking. *Sensors*, 23(6):3018, 2023.

- [77] Kaige Wu, Nobu Yatagai, Kaita Ito, Takayuki Shiraiwa, and Manabu Enoki. Direct evidence of hydrogen bubble evolution as an acoustic emission source in metal corrosion. *Corrosion Science*, 240:112429, 2024.
- [78] ASTM G199-09. Standard guide for electrochemical noise measurement, 2009.
- [79] Mika P Tarvainen, Perttu O Ranta-Aho, and Pasi A Karjalainen. An advanced detrending method with application to hrv analysis. *IEEE transactions on biomedical engineering*, 49(2):172–175, 2002.
- [80] Ugo Bertocci, François Huet, B Jaoul, and Philippe Rousseau. Frequency analysis of transients in electrochemical noise: mathematical relationships and computer simulations. *Corrosion*, 56(7):675–683, 2000.
- [81] Morgan T Smith and Digby D Macdonald. Wavelet analysis of electrochemical noise data. *Corrosion*, 65(7):438–448, 2009.
- [82] Yang Zhao, Ping Liang, Yanhua Shi, Yunxia Zhang, and TAO Yang. The pitting susceptibility investigation of passive films formed on x70, x80, and x100 pipeline steels by electrochemical noise and mott-schottky measurements. *International Journal of Corrosion*, 2015(1):298584, 2015.
- [83] Wei Tan, Boyuan Gou, Xiangdong Ding, Jun Sun, and Ekhard KH Salje. Wild avalanches and mild fluctuations during filiform corrosion of mg in nacl solution. *Physical Review Research*, 5(3):033219, 2023.

Acknowledgements

I would like to thank all my supervisors, Prof. Arjan Mol, Dr. Pooria Pahlavan, Dr. Axel Homborg, and Romain Habiyaremye. Throughout this thesis, they provided invaluable help, feedback, and advice. Prof. Mol and Dr. Homborg's expertise in electrochemistry inspired many of my ideas, while Dr. Pahlavan and Romain Habiyaremye offered extensive explanations, guidance, and suggestions on acoustic emission, which deepened my understanding of the field. I also wish to thank the MSE Electrochemistry Laboratory for providing an excellent experimental platform. Special thanks to my friend Chengkai Sun—every indepth conversation with him has brought new insights, both academically and in life. Special thanks as well to Ziyang Qiu for supporting me, always. I am also grateful to my family for their unwavering support and encouragement. Despite the distance, you have always stood by me unconditionally. Finally, my sincere thanks to all friends and colleagues. Your contributions in both my research and daily life have been crucial. I am deeply grateful for this.